

This discussion paper is/has been under review for the journal Geoscientific Model Development (GMD). Please refer to the corresponding final paper in GMD if available.

Description of a hybrid ice sheet-shelf model, and application to Antarctica

D. Pollard¹ and R. M. DeConto²

¹Earth and Environmental Systems Institute, Pennsylvania State University, University Park, PA, USA

²Department of Geosciences, University of Massachusetts, Amherst, MA, USA

Received: 2 April 2012 – Accepted: 5 April 2012 – Published: 4 May 2012

Correspondence to: D. Pollard (pollard@essc.psu.edu)

Published by Copernicus Publications on behalf of the European Geosciences Union.

GMDD

5, 1077–1134, 2012

Description of a hybrid ice sheet-shelf model

D. Pollard and
R. M. DeConto

[Title Page](#)

[Abstract](#)

[Introduction](#)

[Conclusions](#)

[References](#)

[Tables](#)

[Figures](#)

[⏪](#)

[⏩](#)

[◀](#)

[▶](#)

[Back](#)

[Close](#)

[Full Screen / Esc](#)

[Printer-friendly Version](#)

[Interactive Discussion](#)

Abstract

The formulation of a 3-D ice sheet-shelf model is described. The model is designed for long-term continental-scale applications, and has been used mostly in paleoclimatic studies. It uses a hybrid combination of the scaled Shallow Ice and Shallow Shelf Approximations for ice flow. Floating ice shelves and grounding-line migration are included, with parameterized ice fluxes at grounding lines that allows relatively coarse resolutions to be used. All significant components and parameterizations of the model are described in some detail. Basic results for modern Antarctica are compared with observations, and simulations over the last 5 million yr are shown to be similar to previously published results using an earlier model version. The sensitivity of ice retreat during the last deglaciation to basal sliding coefficients is discussed.

1 Introduction

This paper describes the formulation of a 3-D ice sheet-shelf model, some aspects of which have been included in earlier papers (Pollard and DeConto, 2007, 2009; henceforth PD07, PD09), but many have not. Here, a full model description is presented, including recently added features that are being used in current work (Pollard and DeConto, 2012; henceforth PD12).

Ice dynamics in the model is a heuristic combination of the scaled Shallow Ice Approximation (SIA) equations for interior grounded (vertically shearing) flow, and the Shallow Shelf (or Shelfy Stream) Approximation (SSA) equations for stream or shelf (longitudinal stretching) flow. The Schoof (2007) parameterization is imposed as a condition on ice fluxes at grounding lines, enabling grounding-line migration to be simulated reasonably accurately without the need for much higher resolution (Schoof, 2007). Standard prognostic finite-difference equations predict ice thickness, internal ice temperatures, and the bedrock response under the ice load. An optional coupling with a sediment model, with explicit quarrying/abrasion, transport and deposition of

GMDD

5, 1077–1134, 2012

Description of a hybrid ice sheet-shelf model

D. Pollard and
R. M. DeConto

[Title Page](#)

[Abstract](#)

[Introduction](#)

[Conclusions](#)

[References](#)

[Tables](#)

[Figures](#)

[⏪](#)

[⏩](#)

[◀](#)

[▶](#)

[Back](#)

[Close](#)

[Full Screen / Esc](#)

[Printer-friendly Version](#)

[Interactive Discussion](#)



deformable sediment under the ice, is fully described in Pollard and DeConto (2003, 2007) and is not covered here. There is no explicit basal hydrologic component in the current model.

The model is designed to be feasible for long-term $O(10^7 \text{ yr})$ continental-scale applications. Early model versions without floating ice (SIA only) were applied to paleo Antarctica (DeConto and Pollard, 2003a,b; Pollard and DeConto, 2003, 2005; Pollard et al., 2005; DeConto et al., 2007) and to other ice sheets and times (Herrmann et al., 2003, 2004; Pollard and Kasting, 2004; Horton et al., 2007, 2010; DeConto et al., 2008; Koenig et al., 2011). Other recent applications using the floating shelf component include PD07, PD09, PD12, Alley et al. (2007), Ackert et al. (2011), Fyke et al. (2011), Mackintosh et al. (2011), DeConto et al. (2012) and Gomez et al. (2012). The model has participated in the ISMIP-HEINO, ISMIP-HOM and MISMIP intercomparisons (Pattyn et al., 2008, 2012; Calov et al., 2010), and in the SeaRISE assessment project (http://websrv.cs.umt.edu/isis/index.php/SeaRISE_Assessment).

For reference, new features added to the model since PD09 and described below are listed here:

- new parameterization of oceanic melt at base of floating ice
- calving parameterization at floating ice edge
- sub-grid fractional area of in cells at floating ice edge
- oceanic melting at vertical ice faces
- parameterization of shelf drag by sub-grid bathymetric pinning points
- modified sub-grid application of Schoof (2007) grounding-line condition
- optional simplifications in the combined SIA-SSA dynamics
- adaptive reduction of model timestep to avoid numerical instability

GMDD

5, 1077–1134, 2012

Description of a hybrid ice sheet-shelf model

D. Pollard and
R. M. DeConto

Title Page

Abstract

Introduction

Conclusions

References

Tables

Figures



Back

Close

Full Screen / Esc

Printer-friendly Version

Interactive Discussion

- distribution of basal sliding coefficients deduced by a simple inverse method, described in PD12, and with the resulting pattern used here.

Two other features, not used in the applications below, will be described in future papers:

- sub-grid ice surface elevation interpolation and fractional area for calculation of surface mass balance at terrestrial ice margins (cf. van den Berg et al., 2006)
- improved numerics for nesting model capability in higher-resolution limited domains, with lateral boundary conditions from a previous continental run.

The bulk of this paper (Sects. 2.1 to 2.13) contains the model description, followed by an account of input datasets and climate forcing in Sect. 3. Section 4 presents results for modern Antarctica, where simulations at different resolutions are compared with observations. Section 5 presents paleoclimatic simulations of the last 5 Myrs, repeating those in PD09 with the new model version, and briefly discusses issues concerning the last deglaciation.

2 Model description

The model consists of diagnostic equations for ice velocities, and 3 prognostic equations for the temporal evolution of ice thickness, ice temperature, and bedrock deformation below the ice. Prescribed boundary fields are equilibrium bedrock topography and corresponding loading (modern rebounded ice-free state), unfrozen basal sliding coefficients, geothermal heat flux, and sea level. Monthly mean surface air temperatures and precipitation are either parameterized or provided from a climate model, in order to calculate annual surface mass balance and ice surface temperature (there is no seasonal cycle in the ice model itself). Sub-ice oceanic melting and shelf-edge calving are parameterized for floating ice shelves. A list of model symbols is provided in Table 1.

Description of a hybrid ice sheet-shelf model

D. Pollard and
R. M. DeConto

[Title Page](#)

[Abstract](#)

[Introduction](#)

[Conclusions](#)

[References](#)

[Tables](#)

[Figures](#)



[Back](#)

[Close](#)

[Full Screen / Esc](#)

[Printer-friendly Version](#)

[Interactive Discussion](#)



2.1 Horizontal and vertical grids

The ice sheet-shelf model uses a finite-difference Arakawa-C grid (e.g., Rommelaere and Ritz, 1996), where horizontal velocities (u, v) are calculated on separate grids staggered by half a grid box relative to ice thickness (h), as shown in Fig. 1. The model code contains metric terms appropriate for Cartesian, Polar Stereographic, and Spherical Polar (longitude-latitude) grids, and also for flowlines with one horizontal dimension. Note however that for longitude-latitude grids, a rigorous derivation of the SSA equations introduces some spherical metric terms not in the current code, which would need to be modified in order to properly treat global-scale floating ice (Tziperman et al., 2012).

The ice model uses a vertical coordinate z' running from 0 at the ice surface to 1 at the ice base:

$$z' = (h_s - z)/h$$

where h_s is ice surface elevation and h is ice thickness. The vertical grid has 10 uneven layers, more closely spaced near the top and bottom. Ice temperatures and horizontal velocities are defined at the mid point of each layer.

2.2 Ice velocities

The model heuristically includes vertical shearing, longitudinal stretching and grounding-line migration, while still keeping the numerics simple enough to allow long-term ($O(10^7)$ yr) continental-scale runs. Recent modeling progress using full-Stokes or higher-order flow equations on fine or adaptive grids rigorously include these processes (e.g., Morlighem et al., 2010; Gillet-Chaulet et al., 2011), but require considerably more computer time, and for now are limited to shorter time or smaller spatial scales.

Here, a combination of the scaled equations for shearing ($\partial u/\partial z$, Shallow Ice Approximation, SIA) and stretching ($\partial u/\partial x$, Shallow Shelf Approximation, SSA) is used. The combination is heuristic because neither scaling is accurate where both shearing

GMDD

5, 1077–1134, 2012

Description of a hybrid ice sheet-shelf model

D. Pollard and
R. M. DeConto

[Title Page](#)

[Abstract](#)

[Introduction](#)

[Conclusions](#)

[References](#)

[Tables](#)

[Figures](#)

[⏪](#)

[⏩](#)

[◀](#)

[▶](#)

[Back](#)

[Close](#)

[Full Screen / Esc](#)

[Printer-friendly Version](#)

[Interactive Discussion](#)



and stretching are significant (streaming and grounding zones). Nevertheless, with the additional imposition of Schoof's (2007) grounding-line flux condition described below, results are reasonable in idealized flowline tests and for 3-D modern Antarctica. Analogous non-rigorous combinations have been formulated by Alley and Whillans (1984), van der Veen (1985), Hubbard (1999, 2006), Marshall et al. (2005), Bueler and Brown (2009), and Goldberg (2011).

As described in PD07 and PD09, the SIA and SSA equations are combined by

1. including shear-softening terms in the other's equations,
2. using average horizontal velocity $\bar{u} = \bar{u}_i + u_b$ in the SSA equations, where \bar{u}_i is the vertical mean of the SIA shear flow, and u_b is the basal velocity, and
3. reducing the driving stress in the SIA equations by the gradient of the longitudinal stress from the SSA equations acting on the column above each level.

Symbols are as listed in Table 1. Cartesian coordinates are used in the equations below, although metric terms are included in the model code to handle other grids (but see Sect. 2.1). Note that in a few places later in the paper, “ u ” and “ x ” are written for horizontal velocities and distances, representing “ u or v ”, “ x or y ” as appropriate for 2-D flow. The following presentation of equations is very similar to PD07 Appendix A.

Writing Cartesian horizontal ice velocities as $u(x, y, z)$ and $v(x, y, z)$, define the basal ice velocity $u_b(x, y) = u(x, y, z_b)$, and the internal shearing ice velocity $u_i(x, y, z) = u - u_b$, so that $u_i(x, y, z_b) = 0$. Denoting vertical averages through the ice column with a bar, then $\bar{u} = u_b + \bar{u}_i$ (and similarly for v_b , \bar{v}_i and \bar{v}). The internal shear equations for $u_i(x, y, z)$ and $v_i(x, y, z)$ are

$$\frac{\partial u_i}{\partial z} = 2A \left[\sigma_{xz}^2 + \sigma_{yz}^2 + \sigma_{xx}^2 + \sigma_{yy}^2 + \sigma_{xy}^2 + \sigma_{xx}\sigma_{yy} \right]^{\frac{n-1}{2}} \sigma_{xz} \quad (1a)$$

$$\frac{\partial v_i}{\partial z} = 2A \left[\sigma_{xz}^2 + \sigma_{yz}^2 + \sigma_{xx}^2 + \sigma_{yy}^2 + \sigma_{xy}^2 + \sigma_{xx}\sigma_{yy} \right]^{\frac{n-1}{2}} \sigma_{yz} \quad (1b)$$

Description of a hybrid ice sheet-shelf model

D. Pollard and
R. M. DeConto

Title Page

Abstract

Introduction

Conclusions

References

Tables

Figures



Back

Close

Full Screen / Esc

Printer-friendly Version

Interactive Discussion



Discussion Paper | Discussion Paper | Discussion Paper | Discussion Paper | Discussion Paper

and the horizontal stretching equations for $\bar{u}(x, y)$ and $\bar{v}(x, y)$ are

$$\frac{\partial}{\partial x} \left[\frac{2\mu h}{A^{-1/n}} \left(2\frac{\partial \bar{u}}{\partial x} + \frac{\partial \bar{v}}{\partial y} \right) \right] + \frac{\partial}{\partial y} \left[\frac{\mu h}{A^{-1/n}} \left(2\frac{\partial \bar{u}}{\partial y} + \frac{\partial \bar{v}}{\partial x} \right) \right] \quad (2a)$$

$$= \rho_i g h \frac{\partial h_s}{\partial x} + \frac{f_g}{C^{1/m}} |u_b^2 + v_b^2|^{\frac{1-m}{2m}} u_b$$

$$\frac{\partial}{\partial y} \left[\frac{2\mu h}{A^{-1/n}} \left(2\frac{\partial \bar{v}}{\partial y} + \frac{\partial \bar{u}}{\partial x} \right) \right] + \frac{\partial}{\partial x} \left[\frac{\mu h}{A^{-1/n}} \left(2\frac{\partial \bar{u}}{\partial y} + \frac{\partial \bar{v}}{\partial x} \right) \right] \quad (2b)$$

$$= \rho_i g h \frac{\partial h_s}{\partial y} + \frac{f_g}{C^{1/m}} |u_b^2 + v_b^2|^{\frac{1-m}{2m}} v_b$$

Equations (2a,b) and their horizontal boundary conditions for unconfined ice shelves are derived for instance in Morland (1982) and MacAyeal (1996). In the zero-order shallow ice approximation, the vertical shear stress (σ_{xz} , σ_{yz}) in Eqs. (1a,b) would be balanced only by the hydrostatic driving force $-\rho g(h_s - z)(\partial h_s/\partial x, \partial h_s/\partial y)$ acting on the ice column above level z . Here, horizontal stretching forces are included in this force balance (Hubbard, 1999, 2006; Marshall et al., 2005), so that

$$\sigma_{xz} = - \left(\rho_i g h \frac{\partial h_s}{\partial x} - \text{LHS}_x \right) \left(\frac{h_s - z}{h} \right), \quad \sigma_{yz} = - \left(\rho_i g h \frac{\partial h_s}{\partial y} - \text{LHS}_y \right) \left(\frac{h_s - z}{h} \right) \quad (3)$$

where LHS_x and LHS_y are the left-hand sides of Eqs. (2a) and (2b), respectively. Because horizontal stretching forces are taken to be vertically uniform and the terms in Eq. (2) are forces on the whole ice thickness, their effect on the ice column above level z is scaled by $(h_s - z)/h$ in Eq. (3).

Description of a hybrid ice sheet-shelf model

D. Pollard and
R. M. DeConto

[Title Page](#)

[Abstract](#)

[Introduction](#)

[Conclusions](#)

[References](#)

[Tables](#)

[Figures](#)

[⏪](#)

[⏩](#)

[◀](#)

[▶](#)

[Back](#)

[Close](#)

[Full Screen / Esc](#)

[Printer-friendly Version](#)

[Interactive Discussion](#)



Inclusion of the strain softening terms in Eqs. (1) and (2) due to each other's flow requires manipulation of the constitutive relation for ice rheology. In Eq. (2),

$$\mu \equiv \frac{1}{2} (\dot{\epsilon}^2)^{\frac{1-n}{2n}} \quad (4)$$

and $\bar{A} = \int A dz/h$ is the vertical mean of the Arrhenius temperature-dependent coefficient in the constitutive relation

$$\dot{\epsilon}_{ij} = A(T) (\sigma^2)^{\frac{n-1}{2}} \sigma_{ij} \text{ or equivalently } \dot{\epsilon}_{ij} = A(T)^{\frac{1}{n}} (\dot{\epsilon}^2)^{\frac{n-1}{2n}} \sigma_{ij} \quad (5)$$

where $\dot{\epsilon}_{ij}$ are strain rates, σ_{ij} are deviatoric stresses, and $\dot{\epsilon}$ and σ are the second invariants of their respective tensors. The latter are defined by $\dot{\epsilon}^2 \equiv \sum_{ij} \frac{1}{2} \dot{\epsilon}_{ij} \dot{\epsilon}_{ij}$ and $\sigma^2 \equiv$

$\sum_{ij} \frac{1}{2} \sigma_{ij} \sigma_{ij}$. The relationship

$$\dot{\epsilon}^2 \approx \left(\frac{\partial \bar{u}}{\partial x} \right)^2 + \left(\frac{\partial \bar{v}}{\partial y} \right)^2 + \frac{\partial \bar{u}}{\partial x} \frac{\partial \bar{v}}{\partial y} + \frac{1}{4} \left(\frac{\partial \bar{u}}{\partial x} + \frac{\partial \bar{v}}{\partial y} \right)^2 + \frac{1}{4} \left(\frac{\partial \bar{u}_i}{\partial z} \right)^2 + \frac{1}{4} \left(\frac{\partial \bar{v}_i}{\partial z} \right)^2 \quad (6)$$

is used to set μ in Eq. (2), and follows using

$$\dot{\epsilon}^2 = \dot{\epsilon}_{xx}^2 + \dot{\epsilon}_{yy}^2 + \dot{\epsilon}_{zz}^2 + \dot{\epsilon}_{xx} \dot{\epsilon}_{yy} + \dot{\epsilon}_{xx} \dot{\epsilon}_{zz} + \dot{\epsilon}_{yy} \dot{\epsilon}_{zz},$$

$$\dot{\epsilon}_{xx} + \dot{\epsilon}_{yy} + \dot{\epsilon}_{zz} = 0,$$

$$\dot{\epsilon}_{xx} = \frac{\partial \bar{u}}{\partial x}, \quad \dot{\epsilon}_{yy} = \frac{\partial \bar{v}}{\partial y}, \quad \dot{\epsilon}_{xy} = \frac{1}{2} \left(\frac{\partial \bar{u}}{\partial y} + \frac{\partial \bar{v}}{\partial x} \right), \quad \dot{\epsilon}_{xz} \approx \frac{1}{2} \frac{\partial \bar{u}_i}{\partial z}, \quad \dot{\epsilon}_{yz} \approx \frac{1}{2} \frac{\partial \bar{v}_i}{\partial z}.$$

The corresponding expression for σ^2 is used in Eq. (1), and the purely horizontal components are obtained in our numerical procedure from

$$\sigma_{xx}^2 + \sigma_{yy}^2 + \sigma_{xy}^2 + \sigma_{xx} \sigma_{yy} = \left(\frac{2\mu}{A^{-1/n}} \right)^2 \left[\left(\frac{\partial \bar{u}}{\partial x} \right)^2 + \left(\frac{\partial \bar{v}}{\partial y} \right)^2 + \frac{\partial \bar{u}}{\partial x} \frac{\partial \bar{v}}{\partial y} + \frac{1}{4} \left(\frac{\partial \bar{u}}{\partial x} + \frac{\partial \bar{v}}{\partial y} \right)^2 \right] \quad (7)$$

Description of a hybrid ice sheet-shelf model

D. Pollard and
R. M. DeConto

Title Page

Abstract

Introduction

Conclusions

References

Tables

Figures

⏪

⏩

◀

▶

Back

Close

Full Screen / Esc

Printer-friendly Version

Interactive Discussion

Description of a hybrid ice sheet-shelf model

D. Pollard and
R. M. DeConto

Title Page

Abstract

Introduction

Conclusions

References

Tables

Figures

⏪

⏩

◀

▶

Back

Close

Full Screen / Esc

Printer-friendly Version

Interactive Discussion



The basal sliding relation used on the right-hand sides of Eqs. (2a) and (2b) for grounded ice is $\tilde{u}_b = C|\tau_b|^{m-1}\tilde{\tau}_b$ (see Sect. 2.4), or equivalently $\tilde{\tau}_b = C^{-\frac{1}{m}}|u_b|^{\frac{1-m}{m}}\tilde{u}_b$, where $\tilde{\tau}_b$ is basal stress. Where ice is grounded, i.e., where $\rho_w(S - h_b) < \rho_i h$ or the ocean has no access (held back by intervening thicker ice or higher land), then $f_g = 1$ in the sliding terms, and the ice surface elevation $h_s = h + h_b$. Where ice is floating, i.e., $\rho_w(S - h_b) > \rho_i h$ and the ocean has access, then $f_g = 0$ and $h_s = S + h(1 - \rho_i/\rho_w)$.

At each timestep, an outer iteration is performed that solves for SSA and SIA velocities, updates ice thicknesses for half of the timestep, re-solves the velocities using the new ice thicknesses, etc. In the solution of Eq. (2) for SSA velocities, a standard (Picard) inner iteration is performed to account for the non-linear dependence of μ and basal sliding on the velocities in Eqs. (2), (4) and (6). The outer iteration converges naturally to the appropriate scaling of SSA vs. SIA flow, depending on the magnitude of the basal sliding coefficient. Usually the flow is either almost all vertical shear, with basal drag balancing the driving stress and with negligible stretching, or is almost all longitudinal stretching which balances the driving stress, with small or no basal drag and negligible internal shear. For a fairly narrow range of sliding coefficients, significant amounts of both flow types co-exist.

In each pass of the outer iteration, the SSA Eqs. (2) are solved first, using a Sparse Matrix method, or optionally, Successive-Over-Relaxation (SOR) (or a tridiagonal matrix solution for 1-D flowline problems). Then the ice-thickness advection equation (Sect. 2.6) is time-stepped accounting for both SSA and SIA flow. Advection due to SIA is performed time implicitly, with the vertically averaged SIA flow given from Eqs. (1) and (3) and using time-implicit linearized Newton-Raphson contributions from all h and $\partial h_s/\partial x$ terms (as in earlier SIA-only model versions; DeConto and Pollard, 2003). Centered ice thicknesses are used for the SIA advection, whereas the time-explicit SSA advection uses upstream ice thicknesses for stability. An Alternating Direction Implicit (ADI) scheme is used for x vs. y directions (Mahaffy, 1976). A CFL-based maximum speed limit on \bar{u} can be imposed for stability. No ice advection is allowed *out* of

grid cells with sub-grid areal fraction $f_e < 1$ (which occurs only for cells at the edge of floating ice shelves, see Sect. 2.9).

CPU time in the model is dominated by the Sparse-Matrix (or SOR) solutions of the SSA equations. As described in PD09, a considerable reduction in CPU time can be achieved by restricting the full SSA-SIA iterative procedure to grid points with mid-to-high values of the basal sliding coefficient, $C(x, y) \geq 10^{-8} \text{ ma}^{-1} \text{ Pa}^{-2}$ (see PD12). This range includes all fast streaming regions underlain with deformable sediment ($\sim 10^{-5}$). For lower $C(x, y)$ values $< 10^{-8}$ (including hard bedrock, $\sim 10^{-10}$), the full procedure yields virtually 100% shearing (SIA) flow anyway. At the latter points, advection by internal deformation (\bar{u}_i) and basal sliding (u_b) are both modeled by standard SIA dynamics. At full SSA-SIA points with $C(x, y) \geq 10^{-8}$, advection by SIA internal deformation (\bar{u}_i) is still included, and advection by basal and additional horizontal stretching is represented by the SSA solution \bar{u} minus \bar{u}_i . Tests show that results are essentially unchanged from those with the full SSA-SIA iteration performed at all locations.

In intermediate model versions, some simplifications were tried in the coupling dynamics such as neglecting the strain softening cross-terms in Eqs. (1) and (6), which reduced CPU time modestly with only slight effects on the results. Some of these simplifications were used for the figures shown below; however, the most complete and current model version is described above.

2.3 Grounding-line flux condition

Flowline tests with hybrid or higher-order models show that in order to capture grounding-line migration accurately, it is necessary either to resolve the grounding-zone boundary layer at very fine resolution (Schoof, 2007; Gladstone et al., 2010a; Pattyn et al., 2012), or to apply an analytic constraint on the flux across the grounding line. The latter approach is used here, with flux q_g across model grounding lines

Description of a hybrid ice sheet-shelf model

D. Pollard and
R. M. DeConto

[Title Page](#)

[Abstract](#)

[Introduction](#)

[Conclusions](#)

[References](#)

[Tables](#)

[Figures](#)

[⏪](#)

[⏩](#)

[◀](#)

[▶](#)

[Back](#)

[Close](#)

[Full Screen / Esc](#)

[Printer-friendly Version](#)

[Interactive Discussion](#)



parameterized as in Schoof (2007, his Eq. 29):

$$q_g = \left(\frac{\bar{A} (\rho_i g)^{n+1} (1 - \rho_i / \rho_w)^n}{4^n C_S} \right)^{\frac{1}{m_S+1}} \left(\frac{\tau_{XX}}{\tau_f} \right)^{\frac{n}{m_S+1}} \left(h_g^{\frac{m_S+n+3}{m_S+1}} \right) \quad (8)$$

This yields the vertically averaged velocity $u_g = q_g / h_g$ where h_g is the ice thickness at the grounding line. The middle term in Eq. (8) accounts for back stress at the grounding line due to buttressing by downstream islands, pinning points or side-shear, where τ_{XX} is the longitudinal stress just downstream of the grounding line (τ_{YY} for y -direction), calculated from the viscosity and strains in a preliminary SSA solution with no Schoof constraints. The “free” stress τ_f is the same quantity in the absence of any buttressing, given by $0.5\rho_i g h_g (1 - \rho_i / \rho_w)$ (cf. Goldberg et al., 2009; Gagliardini et al., 2010). A is the depth-averaged ice rheological coefficient and n is the Glen–Law exponent, C_S is Schoof’s (2007) basal sliding coefficient and m_S the basal sliding exponent, corresponding to $C^{-1/m}$ and $1/m$ here, due to the reversed form of the basal sliding law. ρ_i and ρ_w are densities of ice and ocean water, respectively, and g is the gravitational acceleration. h_g is interpolated in space by first estimating the sub-grid position of the grounding line between the two surrounding floating and grounded h -grid points. This is done by linearly interpolating height-above-flotation between those two points to where it is zero, linearly interpolating bedrock elevation to that location, and then simply computing the flotation thickness of ice for that bedrock elevation and current sea level (equivalent to LI in Gladstone et al., 2010b).

The velocity u_g is calculated at the grounding-line points on the u -grid, i.e., those with floating ice in one adjacent (left or right) h -grid box and grounded ice in the other (and similarly for v_g on the v -grid). These velocities are imposed as an internal boundary condition for the flow equations, in effect overriding the large-scale velocity solution at the grounding line. Note that this procedure only considers one-dimensional dynamics perpendicular to the grounding line, as in the 1-D flowline analysis in Schoof (2007). This works naturally with the staggered C-grid (Sect. 2.7), where the grounding “line” is

Description of a hybrid ice sheet-shelf model

D. Pollard and
R. M. DeConto

Title Page

Abstract

Introduction

Conclusions

References

Tables

Figures



Back

Close

Full Screen / Esc

Printer-friendly Version

Interactive Discussion



Description of a hybrid ice sheet-shelf model

D. Pollard and
R. M. DeConto

[Title Page](#)

[Abstract](#)

[Introduction](#)

[Conclusions](#)

[References](#)

[Tables](#)

[Figures](#)

[⏪](#)

[⏩](#)

[◀](#)

[▶](#)

[Back](#)

[Close](#)

[Full Screen / Esc](#)

[Printer-friendly Version](#)

[Interactive Discussion](#)

a continuous series of perpendicular segments of u -direction or v -direction interfaces between h -grid boxes, and u_g (v_g) velocities flow across interfaces running through u -grid (v -grid) points. Spatial gradients parallel to the grounding line, not included in the derivation of Eq. (8), are neglected here (cf. Katz and Worster, 2010). We have tested this method of solution in many idealized 1-D flowline tests, similar to those in Schoof (2007). Our goal was to achieve the same grounding-migration results using a coarse grid (~ 10 to 40 km) with those using very fine-grids (~ 0.1 km). For grids coarser than ~ 1 km, we find that it is necessary to impose Eq. (8) as a grounding-line boundary condition. For grids coarser than a few km, we find that an additional rule is necessary, because the outer-solution structure of the grounding zone is not fully captured by the grid:

If the flux q_g from Eq. (8) is greater than the large – scale shelf – equation's flux q_m at the grounding line, then u_g ($= q_g/h_g$) is imposed exactly at the u – grid grounding – line point; conversely if $q_g < q_m$, then u_g is imposed one u – grid box downstream of the grounding – line point. The former is usually associated with grounding – line retreat, and the latter usually with grounding – line advance.

When converting the grounding-line flux q_g from Eq. (8) to a velocity (u_g), it is important to divide by the ice thickness (called h_g above) that will effectively be used at the relevant point Eq. (9) in the finite-difference numerics of the ice advection equation. Then the model's flux at that point will be exactly that from Eq. (8). In simple equilibrated flowline tests, this means that the model flux equals the net surface mass balance upstream from the grounding line, an important property of analytic solutions. This yields good agreement with analytic solutions including hysteresis in MISMIP-like tests, using grid sizes of ~ 5 to several 10 's km (Pollard and DeConto, 2011; Docquier et al., 2011; Pattyn et al., 2012). The agreement can be made almost exact by adjusting the flux q_g for the increment in surface mass balance between the actual grounding line and the point where Eq. (9) is applied, as illustrated in Fig. 2. The analytic solutions

in turn agree well with full-Stokes model results, at least in steady-state non-transient situations (Drouet et al., 2011; Pattyn et al., 2012).

In efforts to minimize single-cell dithering in some idealized tests, i.e., flipping back and forth between upstream and downstream points in Eq. (9), two further measures were taken:

1. An initial SSA solution is done at each time step, without any imposed flux from Eq. (8), to calculate the large-scale flux that is compared to the imposed flux in step Eq. (9). Previously the large-scale flux was estimated by local finite differences.
2. Values of the imposed velocities from Eq. (8) are calculated for both upstream and downstream points of the grounding line, and these are imposed in the flow equations with weights between 0 and 1 depending on how much (and with what sign) the large-scale flux differs from the imposed flux Eq. (8).

These measures had little effect on the dithering in flowline tests, but fortunately no associated degradation of large-scale results has been detected.

2.4 Basal sliding coefficients

Basal sliding is treated similarly to PD09 by a standard drag law (Cuffey and Paterson, 2010; Pattyn, 2010; Le Brocq et al., 2011)

$$\tilde{u}_b = C' |\tau_b|^{m-1} \tilde{\tau}_b \quad (10)$$

where \tilde{u}_b is basal sliding velocity, $\tilde{\tau}_b$ is basal stress, and $m = 2$ as in Sect. 2.2. As described in PD12, the sliding coefficient C' depends on homologous basal temperature, implicitly representing basal hydrology:

$$C' = (1 - r)C_{\text{froz}} + rC(x, y) \quad \text{where } r = \max[0, \min[1, (T_b + 3)/3]] \quad (11)$$

Description of a hybrid ice sheet-shelf model

D. Pollard and
R. M. DeConto

Title Page

Abstract

Introduction

Conclusions

References

Tables

Figures

⏪

⏩

◀

▶

Back

Close

Full Screen / Esc

Printer-friendly Version

Interactive Discussion



Description of a hybrid ice sheet-shelf model

D. Pollard and
R. M. DeConto

Title Page

Abstract

Introduction

Conclusions

References

Tables

Figures

⏪

⏩

◀

▶

Back

Close

Full Screen / Esc

Printer-friendly Version

Interactive Discussion

isostatically rebounded, 9-point-smoothed bed elevation on the model grid, used to mimic SA in data-sparse regions (PD12). The values of the constants are discussed in PD12. Whitehouse et al. (2012) apply a similar increase in sliding coefficient over mountainous terrain, for much the same reasons. Equation (12) and the associated inverse-derived $C(x, y)$ distribution (Fig. 3b) are used in the simulations below.

For grid points where the full SSA-SIA iteration is performed (Sect. 2.2), u_b enters in the right-hand side of the SSA equations (Eq. 2) (where Eq. (10) is inverted to give τ_b as a function of u_b), and u_b is treated time explicitly in the stepping of the ice-thickness equation. For points where just the SIA equation is used, Eq. (10) is treated time implicitly, with τ_b equal to the driving stress ($\rho_i g h \partial h_s / \partial x$), and linearized Newton-Raphson contributions from Eq. (10) in the same way as for internal shearing (Eq. 1).

2.5 Sub-grid pinning points

Under the major ice shelves, there may be sub-grid pinning points due to small bathymetric rises scraping the bottom of the ice, especially near the grounding line, that are unresolved by the model grid. This is parameterized simply in terms of the standard deviation of observed bathymetry within each model cell. The fractional area f_g of ice in contact with sub-grid bathymetric high spots is

$$f_g = 0.5 \max \left[0, 1 - \frac{h_w}{s_{\text{dev}}} \right] \quad (13)$$

where h_w is the thickness of the ocean column between the cell-mean bedrock and ice base, and s_{dev} is the standard deviation of the observed bed elevations (ALBMAP, 5 km, Le Brocq et al., 2010) within the cell. For 20 to 40 km grids, s_{dev} is typically smaller than ~ 50 m under the Ross and much of the Weddell and Amery ice shelves, but up to a few 100's m in isolated patches of the Weddell, Lambert, and much of Pine Island Bay.

f_g here is identical to the f_g in Eq. (2a,b), and modifies the basal stress for the cell. Instead of no drag ($f_g = 0$, freely floating ice), the value from Eq. (13) is used, increasing

the basal stress to f_g times the amount for 100 % basal contact. In effect, this provides a small buttressing effect and increased grounding-line back pressure for some ice shelves, in addition to the resolved side drag. Its validity should be examined in future work with improving bathymetric data (Timmermann et al., 2010), or possibly by examining small-scale surface features (cf. Horgan and Anandakrishnan, 2006; Hulbe et al., 2010).

2.6 Ice thickness

$$\frac{\partial h}{\partial t} = -\frac{\partial(\bar{u}h)}{\partial x} - \frac{\partial(\bar{v}h)}{\partial y} + \text{SMB} - \text{BMB} - \text{OMB} - \text{CMB} - \text{FMB} \quad (14)$$

where SMB = surface mass balance, BMB = basal melting (if grounded), OMB = oceanic sub-ice melting or freezing (if floating), CMB = calving loss (floating edge), FMB = face melt loss (floating or tidewater vertical face).

The time stepping of the ice thickness equation is done as part of the iterative solution of ice velocities as described in Sect. 2.2. The treatments of the various local ice gains or losses (SMB, etc.) are described in later sections.

2.7 Ice temperature and rheology

The prognostic equation for internal ice temperatures $T(x, y, z', t)$ is

$$\frac{\partial T}{\partial t} = -u \frac{\partial T}{\partial x} - v \frac{\partial T}{\partial y} - w' \frac{\partial T}{\partial z'} + \frac{1}{\rho_i c_i h^2} \frac{\partial}{\partial z'} \left(k_i \frac{\partial T}{\partial z'} \right) + \frac{Q_i}{\rho_i c_i} \quad (15)$$

where $z' = (h_s - z)/h$, $k_i = 2.1 \times 365 \times 86400 \text{ Ja}^{-1} \text{ m}^{-1} \text{ K}^{-1}$ is ice thermal conductivity, and Q_i is internal shear heating ($\vec{\tau} \cdot \vec{u}$) due to both SIA and SSA deformation. Only vertical heat diffusion is included; horizontal heat diffusion is assumed negligible on scaling grounds. The internal velocities u, v, w' (with $w' = dz'/dt$) are calculated by adding the internal SIA shear to the basal velocity (Ritz et al., 1997). The large-scale

Description of a hybrid ice sheet-shelf model

D. Pollard and
R. M. DeConto

Title Page

Abstract

Introduction

Conclusions

References

Tables

Figures

⏪

⏩

◀

▶

Back

Close

Full Screen / Esc

Printer-friendly Version

Interactive Discussion



advective terms $(-u\partial T/\partial x - v\partial T/\partial y - w'\partial T/\partial z')$ are calculated time-explicitly, using upstream parabolic interpolation for T (Farrow and Stevens, 1995).

The upper boundary condition is $T(x, y, 0, t) =$ surface ice temperature, deduced from surface air temperatures (Sect. 3). For grounded ice, the lower boundary condition at the ice base is that the vertical conductive flux $(k_i/h)\partial T/\partial z'$ at $z' = 1$ is equal to the vertical conductive flux at the top of the bedrock (see below) plus any basal shear heating $Q_b = \tilde{\tau}_b \cdot \tilde{u}_b =$; or, if $T(x, y, 1, t)$ would exceed the basal pressure melt point T_m , then it is set equal to T_m and the imbalance in conductive fluxes plus Q_b is used to melt basal ice. For floating ice, the basal boundary condition is simply $T(x, y, 1, t) = T_m$. (Oceanic melt rates are parameterized separately in Sect. 2.8.)

Equation (15) is time-stepped with the vertical diffusive terms and boundary conditions treated time implicitly, which involves a standard tridiagonal solution versus z' for each ice column. To avoid numerical instability, very small ice thicknesses (< 1 m) are treated as a thin film with zero heat capacity, but still with latent heat and melting if its temperature would otherwise exceed the pressure melt point.

Surface melting, refreezing and locally mobile liquid are calculated along with the surface mass balance (Sect. 3). Any locally mobile liquid (rain, snow melt and ice melt, minus refreezing) is assumed to immediately percolate downwards into the local vertical ice column, exchanging its latent heat with the sensible heat of the next lowest layer, i.e., if the layer is below freezing, then some (all) of the percolating liquid freezes, raising the layer temperature to (towards) the pressure melt point (and adding to the layer thickness). If the melt point is reached, the remaining water percolates down to the next layer, and so on. If any liquid reaches the base, it is added to any ice melt at the base itself, and is simply recorded as mass lost to the model (there is no basal hydrologic component).

The model includes vertical heat diffusion and storage in bedrock below the ice, heated from below by a specified geothermal heat flux. Nominally, and in all simulations shown below, its effect is minimized by using a very thin (30 m) single layer, so that the geothermal heat flux is essentially applied to the base of the ice. In other applications,

GMDD

5, 1077–1134, 2012

Description of a hybrid ice sheet-shelf model

D. Pollard and
R. M. DeConto

[Title Page](#)

[Abstract](#)

[Introduction](#)

[Conclusions](#)

[References](#)

[Tables](#)

[Figures](#)

[⏪](#)

[⏩](#)

[◀](#)

[▶](#)

[Back](#)

[Close](#)

[Full Screen / Esc](#)

[Printer-friendly Version](#)

[Interactive Discussion](#)



it is typically ~2 km thick with 6 unequally spaced layers (cf. Ritz et al., 1997). Physical and thermal properties of bedrock are given in Table 1.

In the ice dynamics (Sect. 2.2 and 2.3), the ice rheological coefficient A and its dependence on temperature are specified as in Huybrechts (1998):

$$A = E \times 5.47 \times 10^{10} e^{-13.9 \times 10^4 / (8.314 T')} \quad \text{if } T' \geq 263.15^\circ\text{K} \quad (16a)$$

$$A = E \times 1.14 \times 10^{-5} e^{-6.0 \times 10^4 / (8.314 T')} \quad \text{if } T' < 263.15^\circ\text{K} \quad (16b)$$

where T' is the homologous ice temperature $T - T_m$, where $T_m = -0.000866z$ is the pressure melting point ($^\circ\text{C}$) and z is depth (m) below ice surface. Units of A are $\text{a}^{-1} \text{Pa}^{-3}$ corresponding to $n = 3$ in Eqs. (1) to (7). The enhancement factor E is set to 1 for SIA flow (Eq. 1, see PD12), and to 0.3 for SSA flow (Eqs. 2 and 8). This ratio of enhancement factors is somewhat smaller but not dissimilar to the range 5:1 to 10:1 suggested by Ma et al. (2010). The variation of A vs. z' in the vertical integration of Eq. (1) for SIA flow $u_i(z')$ and \bar{u}_i is treated as in Ritz et al. (1997).

2.8 Sub-ice-shelf oceanic melting

The simulation of oceanic melting at the base of Antarctic ice shelves is challenging, involving incursions of Circumpolar Deep Water (CDW) or High Salinity Shelf Water (HSSW) and other mechanisms that differ from basin to basin (e.g., Nicholls et al., 2009; Walker et al., 2009; Jenkins et al., 2010; Olbers and Hellmer, 2010). Coupling with ice sheet models will ultimately require high-resolution 3-D regional ocean modeling (e.g., Dinniman et al., 2011), especially for paleo and future scenarios. For now, we use a crude parameterization that attempts to provide i) the basic modern spatial distribution, and ii) paleoclimatic variations that yield results in accord with geologic data.

In PD09, the parameterization of modern oceanic melt rates was somewhat ad hoc, based on subtended arcs to open ocean. The new parameterization for modern melt

Description of a hybrid ice sheet-shelf model

D. Pollard and
R. M. DeConto

Title Page

Abstract

Introduction

Conclusions

References

Tables

Figures

⏪

⏩

◀

▶

Back

Close

Full Screen / Esc

Printer-friendly Version

Interactive Discussion



follows recent steps with the PISM-PIK ice sheet model (Martin et al., 2011):

$$\text{OMB} = \frac{K K_T \rho_w c_w}{\rho_i L_f} |T_o - T_f| (T_o - T_f) \quad (17)$$

where OMB is the oceanic melt rate at the floating ice base (ma^{-1}) in Eq. (14), T_o is the specified ocean water temperature, and $T_f = 0.0939 - 0.057 \times 34.5 - 0.000764z$ ($^\circ\text{C}$) is the ocean freezing point at ice-base depth z (m) (Beckmann and Goose, 2003; cf. Jenkins and Bombosch, 1995). The transfer factor $K_T = 5 \times 10^{-7} \times 365 \times 86400 = 15.77 \text{ ma}^{-1} \text{ K}^{-1}$ (as in Martin et al. at $T_o - T_f = 1^\circ\text{C}$), and K is an additional O(1) basin-dependent factor given below. Because the freezing point T_f decreases with depth, the dependence on $T_o - T_f$ means that melt rates tend to be higher at the grounding line as deduced from observations. Unlike Martin et al. (2011), the dependence on temperature difference $T_o - T_f$ is quadratic (Holland et al., 2008).

Here, the ocean temperature T_o is specified differently for various Antarctic sectors, based on observations but mainly aiming to produce realistic modern ice-shelf extents and grounding-line positions. The 4 sectors are delineated by crude latitude and longitude ranges, as follows (with latitudes in $^\circ\text{N}$, longitudes in $^\circ\text{E}$, temperatures in $^\circ\text{C}$, and depths in meters), and also shown in Fig. 4a.

– *Amundsen and Bellingshausen Seas, and Western Peninsula:*

[longitude,latitude] = [–140 to –120, > –77] or [–120 to –90, > –85] or [–90 to –65, > –75].

$T_o - T_f$ depends on depth z , based loosely on profiles in the outer Pine Island Bay with an upper layer of colder fresher water (Jacobs et al., 2011), which may be important for the survival of smaller shelves with shallow grounding lines: $T_o - T_f = 0.5$ for $z < 170$, 3.5 for $z > 680$, joined linearly from 170 to 680 m.

$K = 8$ (large, representing relatively direct access of CDW to these coasts)

– *Weddell embayment:*

Description of a hybrid ice sheet-shelf model

D. Pollard and
R. M. DeConto

Title Page

Abstract

Introduction

Conclusions

References

Tables

Figures

⏪

⏩

◀

▶

Back

Close

Full Screen / Esc

Printer-friendly Version

Interactive Discussion



[longitude, latitude] = [−120 to −90, < −85] or [−90 to −65, < −75] or [−65 to −10, all].

$$T_o = -0.8$$

$$K = 1$$

5 – *East Antarctica:*

[longitude, latitude] = [−10 to 160, all].

$T_o - T_f$ and K are as for the Amundsen/Bellinghausen/W. Peninsula sector, even though ocean profile data in Prydz Bay for instance do not indicate a distinct upper layer as clearly as for Pine Island Bay (Smith et al., 1984).

10 – *Ross embayment:*

[longitude, latitude] = [160 to 180, all] or [−180 to −140, all] or [−140 to −120, < −77].

$$T_o = -1.5$$

$$K = 1$$

15 At this point, T_o and K represent conditions under modern exposed shelves. For the West Antarctic sectors, ocean melt is further reduced based on subtended arc to open ocean A (degrees), i.e., the angle formed by the set of all straight lines from the point in question that reach open ocean without hitting land (as in PD09).

$$T'_o = T_o w_a + (-1.7)(1 - w_a) \quad (18a)$$

20 $K' = K w_a + 1 \times (1 - w_a) \quad (18b)$

where

$$w_a = \max[0, \min[1, (A - 50)/20]] \quad (18c)$$

GMDD

5, 1077–1134, 2012

Description of a hybrid ice sheet-shelf model

D. Pollard and
R. M. DeConto

Title Page

Abstract

Introduction

Conclusions

References

Tables

Figures



Back

Close

Full Screen / Esc

Printer-friendly Version

Interactive Discussion



Description of a hybrid ice sheet-shelf model

D. Pollard and
R. M. DeConto

Title Page

Abstract

Introduction

Conclusions

References

Tables

Figures

⏪

⏩

◀

▶

Back

Close

Full Screen / Esc

Printer-friendly Version

Interactive Discussion

This has the effect of reducing ocean melting for regions mostly surrounded by land. It is found to be necessary in long-term paleo runs (Sect. 5 below) to allow WAIS to regrow after a collapse of all marine ice. After a collapse, the surviving small terrestrial ice caps on Western Antarctic islands must first form thin ice shelves that grow over the interior seaway, coalesce, thicken and become buttressed so as to allow grounding lines to advance out from the islands. Equation (18) can be justified by arguing that interior seaways mostly surrounded by land were more protected from warm water intrusions than the modern coast and embayments. This hypothesis should be tested by regional ocean modeling of the environment following a major WAIS collapse. Equation (18) is not applied to East Antarctica for the ad hoc reason that ocean melting from Eq. (17) needs to penetrate into the Lambert Graben in order to produce reasonable modern grounding line and shelf extents there. A similar parameterization to Eq. (18) is also used to restrict calving (Sect. 2.10).

The above yields the distribution of modern ocean melt rates, shown in Fig. 4b. For paleoclimatic applications, long-term climate variations are parameterized much as in PD09, based on a single weighting parameter w_c set proportional to deep-sea-core $\delta^{18}\text{O}$, plus a slight influence of austral summer insolation:

$$w_c = \max [0, \min [2, 1 + S/85 + 1 \times \log(r\text{CO}_2)/\log(2) + \max[0, 0.1 \Delta Q_{80}/3]]] \quad (19)$$

where S is eustatic sea level relative to modern (meters), set proportional to $\delta^{18}\text{O}$ (Lisiecki and Raymo, 2005) with modern $\delta^{18}\text{O}$ corresponding to 0 m and last-glacial-maximum $\delta^{18}\text{O}$ corresponding to -125 m. ΔQ_{80} is the change in January insolation at 80° S from modern (W m^{-2}) (Laskar et al., 2004). $r\text{CO}_2$ is atmospheric CO_2 in units of preindustrial level (280 ppmv), used mainly for deeper time (pre-Pliocene) experiments. For fixed pre-industrial CO_2 , w_c varies between 0 for glacial maxima, 1 for modern-like climates, and 2 for warmest interglacials. w_c is converted to 3 weights for those 3

climates (each between 0 and 1, summing to 1):

$$w_{lgm} = (1 - w_c), \quad w_{mod} = w_c, \quad w_{hot} = 0 \quad \text{for } 0 \leq w_c \leq 1 \quad (20a)$$

$$w_{lgm} = 0, \quad w_{mod} = (2 - w_c), \quad w_{hot} = (w_c - 1) \quad \text{for } 1 < w_c \leq 2 \quad (20b)$$

5 which are used to alter the ocean temperature and basin factor from Eq. (18):

$$T_o'' = -1.7w_{lgm} + T_o'w_{mod} + 5w_{hot} \quad (21a)$$

$$K'' = K'w_{lgm} + K'w_{mod} + 8w_{hot} \quad (21b)$$

10 Finally, T_o'' and K'' are modified for distal locations, to prevent ice shelves from expanding into the Southern oceans far from Antarctica. This is based on ocean bathymetry ($h_w = \text{sea level} - h_b$), assuming much warmer waters at depths $> \sim 2000$ m, with an additional constraint based on arc-to-open-ocean A to ensure this is not done for deep proximal troughs. The final T_o''' and K''' are used in Eq. (17) in place of T_o and K .

$$T_o''' = T_o''(1 - w_d w_e) + \max[T_o'', T_{dist}]w_d w_e \quad (22a)$$

$$15 \quad K''' = K''(1 - w_d w_e) + 10w_d w_e \quad (22b)$$

where

$$T_{dist} = -0.5w_{lgm} + 5w_{mod} + 8w_{hot} \quad (22c)$$

$$w_d = \max[0, \min[1, (h_w - 1900)/200]] \quad (22d)$$

$$20 \quad w_e = \max[0, \min[1, (A - 150)/20]] \quad (22e)$$

2.9 Sub-grid ice shelf fraction

25 In order for the model to represent vertical tidewater faces, and to avoid whole grid-cell jumps in the advance and retreat of ice shelves, floating ice is allowed to occupy a subgrid fraction of cell area, f_e . This is only applied at ice shelf edges adjacent to open

Description of a hybrid ice sheet-shelf model

D. Pollard and
R. M. DeConto

Title Page

Abstract

Introduction

Conclusions

References

Tables

Figures

⏪

⏩

◀

▶

Back

Close

Full Screen / Esc

Printer-friendly Version

Interactive Discussion



ocean; for interior shelf and all grounded points, $f_e = 1$. The motivation and method here closely follow Albrecht et al. (2011) for the PISM-PIK model.

For floating ice cells adjacent to open ocean, the sub-grid “actual” thickness (within the area f_e) is estimated based on the thickness of adjacent, presumably upstream, ice (Albrecht et al., 2011). All adjacent points are examined, and the maximum of their ice thicknesses (h) are taken, but only if they are grounded, or are floating and not themselves adjacent to open ocean. Furthermore, if grounded, the interpolated thickness at the grounding line is used.

Then this maximum thickness, h_{\max} (m) say, is reduced to allow for “typical” downstream thinning into the cell in question:

$$h_e = \max \left[h_{\max} \max (0.25, e^{(-h_{\max}/100)}), 30, h \right] \quad (23)$$

where the minimum of 30 m avoids very thin shelves, and h_e can also not be less than the current cell-mean thickness h . h_e is the estimated “actual” ice thickness within areal fraction f_e of the cell in question.

Finally, to implicitly conserve ice mass, the fractional area occupied by ice in this cell is reset to

$$f_e = h/h_e \quad (24)$$

where h is the cell-mean thickness h (ice volume divided by cell area). Note that the settings above are only done for floating ice cells adjacent to open ocean, otherwise $f_e = 1$ and $h_e = h$. The variable f_e is used elsewhere in the model to scale quantities that truly depend on area of ice, i.e., surface mass balance and oceanic melting are both multiplied by f_e in the ice thickness evolution equation (Eq. 14). Also, as mentioned in Sect. 2.2, no advective flow of ice is allowed *out* of a cell with $f_e < 1$.

2.10 Calving at ice-shelf edge

There has been considerable recent activity in modeling calving of tidewater glaciers and ice shelves, in part because the extent of floating ice can affect the amount of

Description of a hybrid ice sheet-shelf model

D. Pollard and
R. M. DeConto

[Title Page](#)

[Abstract](#)

[Introduction](#)

[Conclusions](#)

[References](#)

[Tables](#)

[Figures](#)

[⏪](#)

[⏩](#)

[◀](#)

[▶](#)

[Back](#)

[Close](#)

[Full Screen / Esc](#)

[Printer-friendly Version](#)

[Interactive Discussion](#)



back stress (buttressing) at the grounding line, and hence the stability of grounded ice upstream (Scambos et al., 2004). Various mechanisms or triggers have been represented in models, including ice thickness over flotation, penetration of crevasses and surface water, and large-scale stress fields (reviewed by Benn et al., 2007; also for instance Alley et al., 2008; Nick et al., 2010; Levermann et al., 2012), but there is little consensus on the main mechanism or mechanisms.

The calving parameterization here is based on the large-scale stress field, represented by the horizontal divergence of floating ice velocities. It shares the same motivation as earlier studies by Doake et al. (1998) and is similar to the parameterization in PISM-PIK (Martin et al., 2011; Winkelmann et al., 2011; Levermann et al., 2012), but without using principal strains, i.e., with no distinction between along-flow and across-flow strains as in Amundson and Truffer (2010). Inclusion of fracture propagation (e.g., Hulbe et al., 2010; Albrecht and Levermann, 2012), multiple stable states (Levermann et al., 2012) and other calving mechanisms are deferred to future work.

First, the divergence of floating ice shelf points div is calculated as

$$div = \partial u / \partial x + \partial v / \partial y \quad (25)$$

using u and v from the solution of the SSA equations (Eq. 2a,b) above. This is done only for floating grid points with full fractional cover ($f_e = 1$, Sect. 2.9), and propagated by nearest-neighbor value to those on the shelf edge with $f_e < 1$. Then, for points at the shelf edge adjacent to open ocean, the grid-mean calving loss CMB (ma^{-1} , used in Eq. (14)) is set as a weight between two values:

$$CMB = (1 - w_c)30 + w_c 3 \times 10^5 \max(div, 0) h_e / dx \quad (26)$$

where the weight $w_c = \min(1, h_e/200)$. Here, h_e is the sub-grid thickness of ice within fraction f_e (Sect. 2.9), and dx is the grid cell size. All units are meters and years. For thin shelves ($h_e \ll 200$ m), calving is simply weighted towards a constant value of 30 ma^{-1} . For thicker shelves, it is weighted towards a value proportional to divergence div (a^{-1}), but only for positive div .

GMDD

5, 1077–1134, 2012

Description of a hybrid ice sheet-shelf model

D. Pollard and
R. M. DeConto

Title Page

Abstract

Introduction

Conclusions

References

Tables

Figures

⏪

⏩

◀

▶

Back

Close

Full Screen / Esc

Printer-friendly Version

Interactive Discussion



The thickness h_e and grid size dx enter in Eq. (26) because $3 \times 10^5 \max(\text{div}, 0)$ represents the calving rate (i.e., average horizontal speed of erosion of the shelf edge into the interior, U_C in Benn et al., 2007), but CMB here is the rate of volume of ice removed from the cell divided by cell area, so the expression is multiplied by $h_e dx/dx^2$.

The magnitude of the 3×10^5 coefficient (300 km) is reasonable on scaling grounds. For a steady-state edge position, the calving rate ($U_C = 3 \times 10^5 \text{ div}$) must balance the advective ice velocity just upstream of the edge (U_T). For the large West Antarctic shelves, ice velocities change significantly upstream on scales of several 100's km, L_T say, so the divergence at the edge is on the order of U_T divided by L_T . In that case, the parameterized $U_C = 3 \times 10^5 U_T/L_T$, which is the same order as U_T as required for steady state.

CMB is further modified for seaways mostly surrounded by land, represented by the angle subtended to open ocean, A . This quantity is also used to modify oceanic melt (Sect. 2.8, Eq. 18). As discussed in that section, these modifications are needed to allow regrowth of thin shelves in Central West Antarctic seaways following a major WAIS collapse (in contrast to the vigorous calving at the edges of the thicker Ross and Weddell shelves today). It can be motivated by considering the effects of icebergs clogging in the restricted seaways, possibly creating a melange that inhibits further calving, but this needs to be explored by future modeling (cf. Vaughan et al., 2011). The calving loss rate CMB is reduced by

$$\text{CMB}' = \text{CMB} \max [0, \min [1, (A - 70)/20]] \quad (27)$$

The divergence div and calving loss given by Eqs. (26) and (27) are shown in Fig. 5 for a modern nested West Antarctic simulation.

For past climates, calving is reduced for cooler environments, similarly to ocean melt in Sect. 2.8. This is somewhat ad hoc, because the dependence of divergence on calving does not directly depend on temperature, as some of the other mechanisms mentioned above. But we find that calving must be reduced in order to allow grounding

Description of a hybrid ice sheet-shelf model

D. Pollard and
R. M. DeConto

[Title Page](#)

[Abstract](#)

[Introduction](#)

[Conclusions](#)

[References](#)

[Tables](#)

[Figures](#)

[⏪](#)

[⏩](#)

[◀](#)

[▶](#)

[Back](#)

[Close](#)

[Full Screen / Esc](#)

[Printer-friendly Version](#)

[Interactive Discussion](#)



lines to expand as observed during glacial maximum periods.

$$\text{CMB}'' = \text{CMB}'(0 \times w_{\text{lgm}} + 1 \times w_{\text{mod}} + 1 \times w_{\text{hot}}) \quad (28)$$

where w_{lgm} , w_{mod} and w_{hot} are the 3 climate weights corresponding to glacial maxima, modern-like and warm interglacial conditions (as in Sect. 2.8, Eq. 20). We are currently developing an alternative calving parameterization that depends on temperature, which may avoid the questionable dependencies in Eqs. (27) and (28).

2.11 Oceanic melt at vertical faces

The parameterization of sub-grid areal fraction in Sect. 2.9 allows tall vertical ice faces to be in contact with the ocean, including tidewater fronts extending one grid cell from deep grounding lines. Observations at Greenland calving faces show that oceanic melting of the submerged ice front can be up to a few meters per day (Rignot et al., 2010). A parameterization of the actual circulation and melt rates at a vertical face (Motyka et al., 2003) is not yet in the model. As a placeholder for now, we calculate the area of each vertical face in contact with the ocean, and simply apply oceanic sub-ice melt rates from Sect. 2.8 to that area. For any ice cell adjacent to and in contact with open ocean, the vertical extent of submerged ice is

$$\Delta z = \frac{\rho_i}{\rho_w} h_e \quad \text{for floating ice} \quad (29a)$$

$$\Delta z = S - h_b \quad \text{for grounded ice} \quad (29b)$$

where S is sea level and h_b is bed elevation. For each of the (up to 4) neighboring cells with no ice and open ocean, Δz is multiplied by the length of the interface (dx for Cartesian grids) and by that cell's oceanic sub-ice melt (OMB from Sect. 2.8). These are summed, and divided by the cell area (dx^2) to yield the cell-mean loss of ice due to face melting FMB used in Eq. (14).

Description of a hybrid ice sheet-shelf model

D. Pollard and
R. M. DeConto

Title Page

Abstract

Introduction

Conclusions

References

Tables

Figures

⏪

⏩

◀

▶

Back

Close

Full Screen / Esc

Printer-friendly Version

Interactive Discussion

2.12 Bedrock deformation

As in Huybrechts and de Wolde (1999) and Ritz et al. (1997, 2001), the response of the bedrock to the changing ice and ocean load is a combination of time-lagged asthenospheric relaxation towards isostatic equilibrium, and modification of the applied load by the elastic lithosphere. The treatment here exactly follows Huybrechts and de Wolde (1999). The downward deflection w_b of the fully relaxed response (as if the asthenosphere had no lag) is given by

$$D\nabla^4 w_b + \rho_b g w_b = q \quad (30)$$

where $D = 10^{25}$ Nm is the flexural rigidity of the lithosphere, ρ_b is the bedrock (asthenospheric) density and g is gravitational acceleration. A lower value of D ($\sim 10^{23}$ to 10^{24} Nm) can optionally be used for West Antarctica (cf. Stern and ten Brink, 1989). The applied load q is

$$q = \rho_i g h + \rho_w g h_w - \rho_i g h_i^{\text{eq}} - \rho_w g h_w^{\text{eq}} \quad (31)$$

where h is ice thickness, h_w is ocean column thickness, and h^{eq} and h_w^{eq} are their values in the equilibrium state (see below).

Equation (30) is solved by a Green's function method. The response to a point load P (q times area) versus radial distance r is:

$$w_p(r) = \frac{PL^2}{2\pi D} \text{kei}(r/L) \quad (32)$$

where kei is a Kelvin function of zeroth order (Brotchie and Silvester, 1969), and $L = (D/\rho_b g)^{1/4} = 132$ km is a flexural length scale. w_p has significant amplitude within several L -lengths of the point load. The w_p are summed over the individual "point loads" of all grid cells (with $P = q \times \text{cell area}$) to give $w_b(x, y)$, the deflection of the bedrock surface from equilibrium that would occur if the asthenosphere relaxed instantaneously.

Description of a hybrid ice sheet-shelf model

D. Pollard and
R. M. DeConto

Title Page

Abstract

Introduction

Conclusions

References

Tables

Figures

⏪

⏩

◀

▶

Back

Close

Full Screen / Esc

Printer-friendly Version

Interactive Discussion



This is assumed to be proportional to the unbalanced pressure at the top of the asthenosphere due to the load alone (Brotchie and Silvester, 1969). The actual bedrock rate of change is given by

$$\frac{\partial h_b}{\partial t} = -\frac{1}{\tau} (h_b - h_b^{\text{eq}} + w_b) \quad (33)$$

where h_b is current bedrock elevation, h_b^{eq} is its equilibrium value, and τ is 3000 yr.

The equilibrium state (h^{eq} and h_w^{eq} in Eq. (31), h_b^{eq} in Eq. (33)) is taken to be the modern observed, assuming that any Glacial Isostatic Adjustments still to occur from the last deglaciation can be neglected (cf. PD12 Appendix B). Equivalently, at the start of a run, the bedrock model alone can be spun up for several 10 000's yr with all ice removed, and the resulting ice-free equilibrated state can be used to define h_b^{eq} , h_w^{eq} (and $h^{\text{eq}} = 0$).

2.13 Time steps, adaptive time stepping

The main ice-dynamical time step Δt_i (for Eq. 14) is selected for most experiments depending on model resolution, for instance ~ 0.1 to 0.5 yr for 5 to 10 km, ~ 0.5 to 1 yr for 20 km, and 2 to 5 yr for 40 km. There is an option for adaptive time stepping that circumvents numerical instabilities, as follows. A restart file is saved at regular time points during a run (spaced ~ 1000 yr apart typically). If a numerical exception (NaN) occurs or if physically unreasonable values of ice thickness, temperature or velocity are detected, the simulation reverts to the previous time point using the last restart file, and tries again to run through the next 1000 yr with the timestep halved. If an anomaly still occurs during the next 1000 yr, the process is repeated, and is attempted up to 4 times (i.e., with timesteps as small as $2^{-4} \times$ the nominal value) before aborting. If an attempt makes it through the next 1000 yr successfully, the timestep is reset to the nominal value and the run continues on.

For the NetCDF history files, no special action is needed if this adaptive “time-looping” occurs, because the model snapshots have a unique time index and overwrite

GMDD

5, 1077–1134, 2012

Description of a hybrid ice sheet-shelf model

D. Pollard and
R. M. DeConto

[Title Page](#)

[Abstract](#)

[Introduction](#)

[Conclusions](#)

[References](#)

[Tables](#)

[Figures](#)

[⏪](#)

[⏩](#)

[◀](#)

[▶](#)

[Back](#)

[Close](#)

[Full Screen / Esc](#)

[Printer-friendly Version](#)

[Interactive Discussion](#)



Description of a hybrid ice sheet-shelf model

D. Pollard and
R. M. DeConto

[Title Page](#)

[Abstract](#)

[Introduction](#)

[Conclusions](#)

[References](#)

[Tables](#)

[Figures](#)

[⏪](#)

[⏩](#)

[◀](#)

[▶](#)

[Back](#)

[Close](#)

[Full Screen / Esc](#)

[Printer-friendly Version](#)

[Interactive Discussion](#)

any previous snapshot with the same time value. For sequential (ascii) files that contain output at regular intervals, marker records are written that allow a postprocessing program to recognize any time-looping and delete repeated sections as needed. The adaptive-timestepping capability can be convenient near the start of experiments that are initialized to a state far from equilibrium with the boundary conditions (e.g., modern ice sheet and other geologic time periods). In those cases, blowups and adaptive time looping tend to occur in the first few hundred years, after which the model becomes adjusted to the boundary conditions and the run continues normally.

Other components of the model are time-stepped or reset at greater intervals. The various intervals are as follows:

- Ice thickness and dynamics (Eq. 14): Δt_i , depends on resolution as above.
- Ice and bed temperatures (Eq. 15): 50 yr, or Δt_i for 10 km resolution or less.
- Bedrock deformation (Eq. 33): 50 yr.
- Resetting oceanic melt and calving parameterizations (Sects. 2.8 and 2.9): Δt_i .
- Resetting parameterized climate (Sect. 3): 50 yr.
- Resetting climate from global or regional climate models (Sect. 3): 1000 yr.
- Recalculating mass balance on ice surface (Sect. 3): 50 to 100 yr. At intervening times, recalculation is done for any ice points whose elevation changes by more than 50 m.

3 Input datasets and climate forcing

Modern Antarctic input fields are obtained mainly from the ALBMAP v1 dataset at 5 km resolution (Le Brocq et al., 2010). The fields used to determine the equilibrium ice and

bedrock state discussed in Sect. 2.12, with ALBMAP names in parentheses, are ice surface elevation (usrf), bedrock topography (lsrf, topg), and ice thickness (thk).

Either of the two available geothermal heat flux maps (Shapiro and Ritzwoller, 2004 (bheatflx_shapiro); Fox Maule et al., 2005 (bheatflx_fox)) can be used in the model, but as discussed in PD12, these differ considerably from each other on regional scales. Rather than choose one or the other, in the nominal model we specify a simple two-value pattern, with 54.6 mW m^{-2} under EAIS and 70 mW m^{-2} under WAIS. Our results are relatively insensitive to these choices (Pollard et al., 2005; PD12; cf. Pattyn, 2010).

For runs with parameterized climate, observed annual accumulation rate P (van de Berg et al., 2006 (accr)) and surface air temperature T_a (Comiso, 2000 (temp)) are used to calculate modern surface mass budgets, as follows:

1. First, T_a and P are horizontally interpolated to the ice model grid, and vertical lapse rate corrections are applied:

$$T'_a = T_a - \gamma(h_s - h_s^{\text{obs}}) \quad (34a)$$

$$P' = P \times 2^{(T'_a - T_a)/\Delta T} \quad (34b)$$

where $\gamma = 0.0080^\circ\text{C m}^{-1}$, ΔT is 10°C (15°C in some runs), h_s is the model surface elevation and h_s^{obs} is the modern observed elevation interpolated to the ice grid (similarly to Huybrechts, 1998; Ritz et al., 2001).

2. A sinusoidal seasonal cycle is added to T'_a , giving monthly air temperatures with peak-to-peak amplitude 20°C at sea level, increasing linearly with elevation to 30°C at 3000 m, and 30°C above (based roughly on GCM climates in the GENESIS v3 model).
3. A basic Positive Degree Day (PDD) scheme is applied to the monthly cycle, with coefficient 0.005 m of melt per degree day. Monthly precipitation P' is either rain or snow depending on whether monthly air temperature is above or below 0°C . Any melt or rain immediately becomes mobile and percolates into the ice sheet

Description of a hybrid ice sheet-shelf model

D. Pollard and
R. M. DeConto

[Title Page](#)

[Abstract](#)

[Introduction](#)

[Conclusions](#)

[References](#)

[Tables](#)

[Figures](#)

[⏪](#)

[⏩](#)

[◀](#)

[▶](#)

[Back](#)

[Close](#)

[Full Screen / Esc](#)

[Printer-friendly Version](#)

[Interactive Discussion](#)



and precipitation to the interpolation and PDD schemes in steps 1 and 3 above (e.g., DeConto and Pollard, 2003; Koenig et al. 2011; DeConto et al., 2011), or provides its own annual surface mass budgets calculated with full climate-model physics directly to the ice model.

4 Modern results

In this section, some basic model results for present-day Antarctica are compared with observations. These simulations have been run to equilibrium with the modern climate, so the comparison ignores any remaining Glacial Isostatic Adjustments in the real world, which are relatively small compared to modern biases (PD12). As discussed in PD12, further work is planned with transient runs through the last deglaciation and extensive comparisons with paleo data (following Briggs, et al., 2011; Whitehouse et al., 2012).

Figure 6 compares ice surface elevations h_s with observed, using the model with parameterized modern climate (Sect. 3) and inverse-derived basal sliding coefficients $C(x,y)$ (Sect. 2.4). Due mainly to the inverse-derived $C(x,y)$, model elevations are within a few 10's m of observed in most regions. Over the Transantarctics and some other mountain ranges, there are small patches with elevations a few hundred meters too high. As discussed in PD12, these are thought to be due to insufficient sliding through deep troughs cutting through the mountains, only partially compensated by the sub-grid topographic parameterization in Eq. (12); however, further work is needed to test that hypothesis.

Much the same level of accuracy in h_s is maintained at different resolutions (20 km and 40 km in Fig. 6; 10 km nested in PD12), which is somewhat surprising for regions such as the Siple Coast with ice streams that are scarcely resolved at 40 km. Apparently the proto-streaming at 20 and 40 km does capture basic features such as interleaved unfrozen vs. frozen beds (Fig. 7), and provides the correct overall flux to the grounding line. (At 10 km resolution, individual Siple Coast ice streams are simulated

Description of a hybrid ice sheet-shelf model

D. Pollard and
R. M. DeConto

[Title Page](#)

[Abstract](#)

[Introduction](#)

[Conclusions](#)

[References](#)

[Tables](#)

[Figures](#)



[Back](#)

[Close](#)

[Full Screen / Esc](#)

[Printer-friendly Version](#)

[Interactive Discussion](#)



quite realistically, including century time-scale rerouting and stagnating; PD09 Supp. Inf.)

As shown in Fig. 7, basal temperatures are also insensitive to model resolution, and agree reasonably well with other work (e.g., Pattyn, 2010). As noted in PD12, the pattern of basal freezing vs. melting beds is relatively insensitive to most moderate model variations, including the choice of geothermal heat flux map.

The model grounding line positions, ice shelf thicknesses and extents are the combined result of the model's SSA-SIA dynamics, grounding-line-flux prescription, and sub-ice oceanic melt, calving and sub-grid pinning parameterizations described above. They are not completely independent of model resolution (Figs. 6 and 7), but the effects of resolution are minor and considerably smaller than other model uncertainties. The major Ross and Filchner-Ronne shelves and grounding lines are reasonably realistic, except that the Ronne grounding line has retreated about 200 km too far south (roughly between the Ellsworth Mountains and the Foundation Ice Stream), causing a pronounced low patch in Fig 6c and f. Other smaller-scale grounding-line errors are seen in Pine Island Bay, Lambert Graben, and especially on the Western Peninsula where George VI Sound (between Alexander Island and the mainland) is overridden with thick grounded ice in the model. The latter errors may require higher-resolution modeling and/or coupling with ocean models to correct entirely, but apart from George VI Sound, the errors are not huge and basic regional features are captured.

The modern bedrock elevations are also quite close to observed over most regions, showing that the bedrock model in Sect. 2.12 is reasonably realistic (Fig. 8). The largest differences are caused by two main grounding-line errors mentioned above, on the Ronne coast and George VI Sound. However, as discussed in PD12 (their Appendix A), some of the general agreement may be fortuitous because the model has not taken transient residuals from the last deglaciation into account. This will be examined further in future work with transient simulations as mentioned above.

The recent all-Antarctic dataset of surface velocities (Rignot et al., 2011) provides the opportunity to comprehensively test the model velocity field, as shown in Fig. 9

GMDD

5, 1077–1134, 2012

Description of a hybrid ice sheet-shelf model

D. Pollard and
R. M. DeConto

[Title Page](#)

[Abstract](#)

[Introduction](#)

[Conclusions](#)

[References](#)

[Tables](#)

[Figures](#)



[Back](#)

[Close](#)

[Full Screen / Esc](#)

[Printer-friendly Version](#)

[Interactive Discussion](#)



Description of a hybrid ice sheet-shelf model

D. Pollard and
R. M. DeConto

[Title Page](#)

[Abstract](#)

[Introduction](#)

[Conclusions](#)

[References](#)

[Tables](#)

[Figures](#)

[⏪](#)

[⏩](#)

[◀](#)

[▶](#)

[Back](#)

[Close](#)

[Full Screen / Esc](#)

[Printer-friendly Version](#)

[Interactive Discussion](#)

where the dataset (900 m spacing) has been regridded by simple area-averaging to the model's 20 km grid. Quantitative comparison is hindered by the fine scale and sharp gradients of many features in the dataset such as numerous outlet glaciers around the coast, many of which are barely resolved by the model and may be slightly displaced to one side or the other. Model speeds in the flanks around most coastlines are generally too fast, both in outlet glaciers and in the slower flow between them. The model's marginal ice thicknesses are generally close to observed (Fig. 6), so the discrepancy might be caused by too much snowfall near the coasts, or too much internal deformation compared to sliding. The biggest single velocity error in Fig. 9 is due to the Kamb Ice Stream (Ice Stream C) on the Siple Coast, which stagnated about 150 yr ago (Hulbe and Fahnestock, 2007), but in the model is flowing at velocities comparable to the other active Ross ice streams.

5 Past 5 Myr results, and last deglaciation issues

In previous Antarctic applications, the model simulated glacial-interglacial variations in the Pliocene and Pleistocene that are in basic accord with observations (PD09). This includes reasonable first-order agreement with grounding-line retreat during the last deglaciation (last ~ 20 kyrs) (PD09 Supp. Inf.), and with surface elevation histories deduced from field data in the Ohio Range (Ackert et al., 2011; Mukhopadhyay et al., 2012).

The applications in PD09 and Ackert et al. (2011) used an earlier model version with a simple two-value specification of basal sliding coefficients (10^{-10} and $10^{-6} \text{ ma}^{-1} \text{ Pa}^{-2}$, Sect. 2.4, Fig. 3a). We repeated the simulations over the last 5 Myrs in PD09 with the current model including the new inverse-derived $C(x, y)$ distribution, and with $C(x, y) = 10^{-5} \text{ ma}^{-1} \text{ Pa}^{-2}$ (maximum value, slippery sediment) specified for all modern ocean beds. As shown in Fig. 10, the results have the same basic features, with predominantly collapsed WAIS in the warm Pliocene, transitioning to larger glacial-

interglacial cycles in the Pleistocene, and rarer WAIS collapses in a few Pleistocene interglacials.

However, the maximum glacial ice volumes are less in the current model, $\sim 29 \times 10^6 \text{ km}^3$ compared to $\sim 33 \times 10^6 \text{ km}^3$ in PD09. This is probably due to greater extents of slipperier beds in the new version (PD09 Supp. Inf. Fig. S7A showed much the same effect). Consequently, the equivalent eustatic sea level rise predicted between the Last Glacial Maximum (LGM) and today is only +1.6 m in the new version (3.5 from WAIS, -1.9 from EAIS due to increasing snowfall), compared to +12 m in PD09. These differences in LGM volume are mainly due to thinner ice on the continental shelves and parts of West Antarctica in the current model (Fig. 11). The different ice thicknesses around the margins affect the timing of grounding-line retreat in the major embayments, and simulated Relative Sea Level curves. As mentioned above, we plan to address these issues in upcoming work with transient simulations and model-data comparisons through the last deglaciation. One focus will be the best-fit values of basal sliding coefficients on the continental shelves (cf. Whitehouse et al., 2012).

6 Conclusions

This paper has described the formulation of a 3-D ice sheet-shelf model, and presented basic validation vs. modern Antarctica. Ice dynamics in the model uses a hybrid combination of the scaled SSA and SIA equations. A parameterization of ice flux across grounding lines (Schoof, 2007) allows grounding-line migration to be captured well, even with coarse (10 to 40 km) grid resolutions. Dynamical tests vs. higher-order models will continue to be important to verify grounding-line behavior, as the model is applied to different domains and scenarios. The model can feasibly be run on continental scales and million-year time scales. Its modern Antarctic ice distributions are reasonably realistic, due in part to an inverse-derived distribution of basal sliding coefficients.

Although the current parameterizations of sub-ice-shelf melting and calving around Antarctica yield reasonable modern and paleoclimatic results, some aspects are ad-

Description of a hybrid ice sheet-shelf model

D. Pollard and
R. M. DeConto

[Title Page](#)

[Abstract](#)

[Introduction](#)

[Conclusions](#)

[References](#)

[Tables](#)

[Figures](#)

[⏪](#)

[⏩](#)

[◀](#)

[▶](#)

[Back](#)

[Close](#)

[Full Screen / Esc](#)

[Printer-friendly Version](#)

[Interactive Discussion](#)



hoc and not well constrained by underlying physics. Planned future work includes improved modeling of ocean circulation and ice melting beneath ice shelf cavities, extending the box model of Olbers and Hellmer (2010), and later coupling with regional ocean models. Further exploration of ice-shelf calving models is anticipated, addressing the need in Plio-Pleistocene simulations to allow re-advance of grounding lines across deep seaways in central West Antarctica after a complete collapse of marine ice. This first requires growth and merging of ice shelves spanning the seaways, which requires calving to be suppressed, despite conditions similar to those at the edges of modern shelves.

Acknowledgements. This research was funded by the US National Science Foundation under awards ANT 0424589, 1043018, 25-0550-0001, and OCE-1202632.

References

- Ackert Jr., R. P., Mukhopadhyay, S., Pollard, D., DeConto, R. M., Putnam, A. E., and Borns Jr., H. W.: West Antarctic Ice Sheet elevations in the Ohio Range: geologic constraints and ice sheet modeling prior to the last highstand, *Earth Planet. Sc. Lett.*, 307, 83–93, 2011.
- Albrecht, T. and Levermann, A.: Fracture field for large-scale ice dynamics, *J. Glaciol.*, 58, 165–176, doi:10.3189/2012JOG11J191, 2012.
- Albrecht, T., Martin, M., Haseloff, M., Winkelmann, R., and Levermann, A.: Parameterization for subgrid-scale motion of ice-shelf calving fronts, *The Cryosphere*, 5, 35–44, doi:10.5194/tc-5-35-2011, 2011.
- Alley, R. B. and Whillans, I. M.: Response of the East Antarctic Ice Sheet to sea-level rise, *J. Geophys. Res.*, 89, 6487–6493, 1984.
- Alley, R. B., Anandakrishnan, S., Dupont, T. K., Parizek, B. R., and Pollard, D.: Effect of sedimentation on ice-sheet grounding-line stability, *Science*, 315, 1838–1841, 2007.
- Alley, R. B., Horgan, H. J., Joughin, I., Cuffey, K. M., Dupont, T. K., Parizek, B. R., Anandakrishnan, S., and Bassis, J.: A simple law for ice-shelf calving, *Science*, 322, 1344, 2008.
- Amundson, J. and Truffer, M.: A unifying framework for iceberg-calving models, *J. Glaciol.*, 56, 822–830, 2010.

Description of a hybrid ice sheet-shelf model

D. Pollard and
R. M. DeConto

Title Page

Abstract

Introduction

Conclusions

References

Tables

Figures



Back

Close

Full Screen / Esc

Printer-friendly Version

Interactive Discussion



Description of a hybrid ice sheet-shelf model

D. Pollard and
R. M. DeConto

[Title Page](#)

[Abstract](#)

[Introduction](#)

[Conclusions](#)

[References](#)

[Tables](#)

[Figures](#)

[⏪](#)

[⏩](#)

[◀](#)

[▶](#)

[Back](#)

[Close](#)

[Full Screen / Esc](#)

[Printer-friendly Version](#)

[Interactive Discussion](#)



- Benn, D. I., Warren, C. R., and Mottram, R. H.: Calving processes and the dynamics of calving glaciers, *Earth-Sci. Rev.*, 82, 143–179, 2007.
- Briggs, R., Pollard, D., and Tarasov, L.: Past evolution of the Antarctic Ice Sheet: a Bayesian calibrated 3-D glacial system modeling study, Abstract PS19.9, Programme and Abstracts, 11th International Symposium on Antarctic Earth Sciences, 10–16 July 2011, Edinburgh, Scotland, 246, 2011.
- Beckmann, A. and Goose, H.: A parameterization of ice shelf-ocean interaction for climate models, *Ocean Model.*, 5, 157–170, 2003.
- Brotchie, J. F. and Silvester, R.: On crustal flexure, *J. Geophys. Res.*, 74, 22, 5240–5252, 1969.
- Bueler, E. and Brown, J.: Shallow shelf approximation as a “sliding law” in a thermomechanically coupled ice sheet model, *J. Geophys. Res.*, 114, F03008, doi:10.1029/2008JF001179, 2009.
- Calov, R., Greve, R., Abe-Ouchi, A., Bueler, E. L., Huybrechts, P., Johnson, J. V., Pattyn, F., Pollard, D., Ritz, C., Saito, F., and Tarasov, L.: Results from the Ice Sheet Model Intercomparison Project – Heinrich Event INterCOmparison (ISMIP HEINO), *J. Glaciol.*, 56, 371–383, 2010.
- Comiso, J. C.: Variability and trends in Antarctic surface temperatures from in situ and satellite infrared measurements, *J. Climate*, 13(10), 1674–1696, 2000.
- Cuffey, K. M. and Paterson, W. S. B.: *The Physics of Glaciers*, 4th edn., Academic Press, Amsterdam, 704 pp., 2010.
- DeConto, R. M. and Pollard, D.: Rapid Cenozoic glaciation of Antarctica induced by declining atmospheric CO₂, *Nature*, 421, 245–249, 2003a.
- DeConto, R. M. and Pollard, D.: A coupled climate-ice sheet modeling approach to the early Cenozoic history of the Antarctic ice sheet, *Palaeogeogr. Palaeocl.*, 198, 39–52, 2003b.
- DeConto, R., Pollard, D., and Harwood, D.: Sea ice feedback and Cenozoic evolution of Antarctic climate and ice sheets, *Paleoceanography*, 22, PA3214, doi:10.1029/2006PA001350, 2007.
- DeConto, R. M., Pollard, D., Wilson, P., Palike, H., Lear, C., and Pagani, M.: Thresholds for Cenozoic bipolar glaciation, *Nature*, 455, 653–656, 2008.
- DeConto, R. M., Pollard, D., and Kowalewski, D.: Past and future vulnerability of the West Antarctic Ice Sheet to surface ice-shelf melt, American Geophysical Union Fall Meeting, 4–9 December 2011, San Francisco, California, USA, Abstract C42A-06, 2011.
- DeConto, R. M., Pollard, D., and Kowalewski, D.: 2012. Modeling Antarctic ice sheet and climate variations during Marine Isotope Stage 31, *Global Planet. Change*, in press, 2012.

Description of a hybrid ice sheet-shelf model

D. Pollard and
R. M. DeConto

[Title Page](#)

[Abstract](#)

[Introduction](#)

[Conclusions](#)

[References](#)

[Tables](#)

[Figures](#)

[⏪](#)

[⏩](#)

[◀](#)

[▶](#)

[Back](#)

[Close](#)

[Full Screen / Esc](#)

[Printer-friendly Version](#)

[Interactive Discussion](#)



Dinniman, M. S., Klinck, J. M., and Smith Jr., W. O.: A model study of Circumpolar Deep Water on the West Antarctic Peninsula and Ross Sea continental shelves, *Deep-Sea Res. Pt. II*, 58, 1508–1523, 2011.

Doake, C. S. M., Corr, H. F. J., Rott, H., Skvarca, P., and Young, N. W.: Breakup and conditions for stability of the Northern Larsen Ice Shelf, *Antarctica, Nature*, 391, 778–780, 1998.

Docquier, D., Perichon, L., and Pattyn, F.: Representing grounding line dynamics in numerical ice sheet models: recent advances and outlook, *Surv. Geophys.*, 32, 417–435, 2011.

Drouet, A.-S., Durand, G., Favier, L., Peyaud, V., Gagliardini, O., Ritz, C., Zwinger, T., and Le Meur, E.: Testing the validity of the boundary layer flux-thickness relationship at the grounding line, *Geophysical Research Abstracts*, vol. 13, EGU2011-3149-1, European Geosciences Union General Assembly, Vienna, Austria, 2011.

Farrow, D. E. and Stevens, D. P.: A new tracer advection scheme for Bryan and Cox type ocean general circulation models, *J. Phys. Oceanogr.*, 25, 1731–1741, 1995.

Fox Maule, C., Purucker, M. E., Olsen, N., and Mosegaard, K.: Heat flux anomalies in Antarctica revealed by satellite magnetic data, *Science*, 309, 464–467, 2005.

Fyke, J. G., Weaver, A. J., Pollard, D., Eby, M., Carter, L., and Mackintosh, A.: A new coupled ice sheet/climate model: description and sensitivity to model physics under Eemian, Last Glacial Maximum, late Holocene and modern climate conditions, *Geosci. Model Dev.*, 4, 117–136, doi:10.5194/gmd-4-117-2011, 2011.

Gagliardini, O., Durand, G., Zwinger, T., Hindmarsh, R. C. A., and Le Meur, E.: Coupling of ice-shelf melting and buttressing is a key process in ice-sheets dynamics, *Geophys. Res. Lett.*, 37, L14501, doi:10.1029/2010GL043334, 2010.

Gillet-Chaulet, F., Gagliardini, O., Nodet, M., Ritz, C., Durand, C., Zwinger, T., Seddick, H., and Greve, R.: Investigating Greenland Ice Sheet dynamics over next century using high resolution full-Stokes simulations, *American Geophysical Union Fall Meeting*, 4–9 December 2011, San Francisco, California, USA, Abstract C42A-07, 2011.

Gladstone, R. M., Lee, V., Vieli, A., and Payne, A. J.: Grounding line migration in an adaptive mesh ice sheet model, *J. Geophys. Res.*, 115, F04014, doi:10.1029/2009JF001615, 2010a.

Gladstone, R. M., Payne, A. J., and Cornford, S. L.: Parameterising the grounding line in flow-line ice sheet models, *The Cryosphere*, 4, 605–619, doi:10.5194/tc-4-605-2010, 2010b.

Goldberg, D. N.: A variationally derived, depth-integrated approximation to a higher-order glaciological flow model, *J. Glaciol.*, 57, 201, 157–170, 2011.

Description of a hybrid ice sheet-shelf model

D. Pollard and
R. M. DeConto

[Title Page](#)

[Abstract](#)

[Introduction](#)

[Conclusions](#)

[References](#)

[Tables](#)

[Figures](#)

[⏪](#)

[⏩](#)

[◀](#)

[▶](#)

[Back](#)

[Close](#)

[Full Screen / Esc](#)

[Printer-friendly Version](#)

[Interactive Discussion](#)



- Goldberg, D. N., Holland, D. M., and Schoof, C.: Grounding line movement and ice shelf buttressing in marine ice sheets, *J. Geophys. Res.*, 114, F04026, doi:10.1029/2008JF001227, 2009.
- 5 Gomez, N., Pollard, D., Mitrovica, J. X., Huybers, P., and Clark, P. U.: Evolution of a coupled marine ice sheet-sea level model, *J. Geophys. Res.-Earth*, 117, F01013, doi:10.1029/2011JF002128, 2012.
- Herrmann, A. D., Patzkowsky, M. E., and Pollard, D.: Obliquity forcing with 8–12x pre-industrial levels of atmospheric $p\text{CO}_2$ during the late Ordovician glaciation, *Geology*, 31, 6, 485–488, 2003.
- 10 Herrmann, A. D., Patzkowsky, M. E., and Pollard, D.: The impact of paleogeography, $p\text{CO}_2$, poleward ocean heat transport and sea level change on global cooling during the late Ordovician, *Palaeogeogr. Palaeoclimatol.*, 206, 59–74, 2004.
- Holland, P. R., Jenkins, A., and Holland, D. M.: The response of ice shelf basal melting to variations in ocean temperature, *J. Climate*, 21, 2558–2572, 2008.
- 15 Horgan, H. J. and Anandakrishnan, S.: Static grounding lines and dynamic ice streams: evidence from the Siple Coast, West Antarctica, *Geophys. Res. Lett.*, 33, L18502, doi:10.1029/2006GL027091, 2006.
- Horton, D. E., Poulsen, C. J., and Pollard, D.: Orbital and CO_2 forcing of late Paleozoic continental ice sheets, *Geophys. Res. Lett.*, 34, L19708, doi:10.1029/2007GL031188, 2007.
- 20 Horton, D. E., Poulsen, C. J., and Pollard, D.: Influence of high-latitude vegetation feedbacks on late Paleozoic glacial cycles, *Nat. Geosci.*, 3, 572–577, 2010.
- Hubbard, A.: High-resolution modeling of the advance of the Younger Dryas ice sheet and its climate in Scotland, *Quaternary Res.*, 52, 27–43, 1999.
- Hubbard, A.: The validation and sensitivity of a model of the Icelandic ice sheet, *Quaternary Sci. Rev.*, 25, 2297–2313, 2006.
- 25 Hulbe, C. and Fahnestock, M.: Century-scale discharge stagnation and reactivation of the Ross ice streams, West Antarctica, *J. Geophys. Res.*, 112, F03S27, doi:10.1029/2006JF000603, 2007.
- Hulbe, C. L., LeDoux, C., and Cruikshank, K.: Propagation of long fractures in the Ronne Ice Shelf, Antarctica, investigated using a numerical model of fracture propagation, *J. Glaciol.*, 56(197), 459–472, 2010.
- 30 Huybrechts, P.: Report of the Third EISMINT Workshop on Model Intercomparison, European Science Foundation, Strasbourg, 140 pp., 1998.

Description of a hybrid ice sheet-shelf model

D. Pollard and
R. M. DeConto

[Title Page](#)

[Abstract](#)

[Introduction](#)

[Conclusions](#)

[References](#)

[Tables](#)

[Figures](#)

[⏪](#)

[⏩](#)

[◀](#)

[▶](#)

[Back](#)

[Close](#)

[Full Screen / Esc](#)

[Printer-friendly Version](#)

[Interactive Discussion](#)



- Huybrechts, P. and de Wolde, J.: The dynamic response of the Greenland and Antarctic ice sheets to multiple-century climatic warming, *J. Climate*, 1, 2169–2188, 1999.
- Jacobs, S. S., Jenkins, A., Giulivi, C. F., and Dutrieux, P.: Stronger ocean circulation and increased melting under Pine Island Glacier ice shelf, *Nat. Geosci.*, 4, 519–523, 2011.
- 5 Jenkins, A. and Bombosch, A.: Modeling the effects of frazil ice crystals on the dynamics and thermodynamics of ice shelf water plumes, *J. Geophys. Res.*, 100, C4, 6967–6981, 1995.
- Jenkins, A., Dutrieux, P., Jacobs, S. S., McPhail, S. D., Perrett, J. R., Webb, A. T., and White, D.: Observations beneath Pine Island Glacier in West Antarctica and implications for its retreat, *Nat. Geosci.*, 3, 468–472, 2010.
- 10 Katz, R. F. and Worster, M. G.: Stability of ice-sheet grounding lines, *P. R. Soc. A*, 466, 1597–1620, doi:10.1098/rspa.2009.0434, 2010.
- Koenig, S. J., DeConto, R. M., and Pollard, D.: Late Pliocene to Pleistocene sensitivity of the Greenland Ice Sheet in response to external forcing and internal feedbacks, *Clim. Dynam.*, 37, 1247–1268. 2011.
- 15 Laskar, J., Robutel, P., Joutel, F., Gastineau, M., Correia, A. C. M., and Levrard, B.: A long-term numerical solution for the insolation quantities of the Earth, *Astron. Astrophys.*, 428, 261–285, 2004.
- Le Brocq, A. M., Payne, A. J., and Vieli, A.: An improved Antarctic dataset for high resolution numerical ice sheet models (ALBMAP v1), *Earth Syst. Sci. Data*, 2, 247–260, doi:10.5194/essd-2-247-2010, 2010.
- 20 Le Brocq, A. M., Bentley, M. J., Hubbard, A., Fogwill, C. J., Sugden, D. E., and Whitehouse, P. L.: Reconstructing the Last Glacial Maximum ice sheet in the Weddell Sea embayment, Antarctica, using numerical modeling constrained by field evidence, *Quaternary Sci. Rev.*, 30, 2422–2432, 2011.
- 25 Levermann, A., Albrecht, T., Winkelmann, R., Martin, M. A., Haseloff, M., and Joughin, I.: Kinematic first-order calving law implies potential for abrupt ice-shelf retreat, *The Cryosphere*, 6, 273–286, doi:10.5194/tc-6-273-2012, 2012.
- Lisiecki, L. E. and Raymo, M.: A Pliocene-Pleistocene stack of 57 globally distributed benthic $\delta^{18}\text{O}$ records, *Paleoceanography*, 20(1), 1–17, 2005.
- 30 Ma, Y., Gagliardini, O., Ritz, C., Gillet-Chaulet, F., Durand, G., and Montagnat, M.: Enhancement factors for grounded ice and ice shelves inferred from an anisotropic ice-flow model, *J. Glaciol.*, 56, 805–812, 2010.

Description of a hybrid ice sheet-shelf model

D. Pollard and
R. M. DeConto

[Title Page](#)

[Abstract](#)

[Introduction](#)

[Conclusions](#)

[References](#)

[Tables](#)

[Figures](#)

[⏪](#)

[⏩](#)

[◀](#)

[▶](#)

[Back](#)

[Close](#)

[Full Screen / Esc](#)

[Printer-friendly Version](#)

[Interactive Discussion](#)



- MacAyeal, D. R.: EISMINT: Lessons in Ice-Sheet Modeling, Dept. of Geophysical Sciences, Univ. of Chicago, 428 pp., geosci.uchicago.edu/pdfs/macayeal/lessons.pdf, 1996.
- Mackintosh, A., Golledge, N., Domack, E., Dunbar, R., Leventer, A., White, D., Pollard, D., DeConto, R. M., Fink, D., Zwartz, D., Gore, D., and Lavoie, C.: Retreat of the East Antarctic ice sheet during the last glacial termination, *Nat. Geosci.*, 4, 195–202, 2011.
- Mahaffy, M. W.: A three-dimensional numerical model of ice sheets: tests on the Barnes Ice Cap, Northwest Territories, *J. Geophys. Res.*, 81(6), 1059–1066, 1976.
- Marshall, S. J., Pollard, D., Hostetler, S., and Clark, P. U.: Coupling ice-sheet and climate models for simulation of former ice sheets, in: *The Quaternary Period in the United States, Developments in Quaternary Science*, vol. 1, edited by: Gillespie, A. R., Porter, S. C., and Atwater, B. F., Elsevier, Amsterdam, 105–126, 2004.
- Marshall, S. J., Bjornsson, H., Flowers, G. E., and Clarke, G. K. C.: Simulation of Vatnajokull ice cap dynamics, *J. Geophys. Res.*, 110, F03009, doi:10.1029/2004JF000262, 2005.
- Martin, M. A., Winkelmann, R., Haseloff, M., Albrecht, T., Bueler, E., Khroulev, C., and Levermann, A.: The Potsdam Parallel Ice Sheet Model (PISM-PIK) – Part 2: Dynamic equilibrium simulation of the Antarctic ice sheet, *The Cryosphere*, 5, 727–740, doi:10.5194/tc-5-727-2011, 2011.
- Morland, L. W.: Unconfined ice-shelf flow, in: *Dynamics of the West Antarctic Ice Sheet*, edited by: van der Veen, C. J. and Oerlemans, J., Springer, New York, 99–116, 1987.
- Morlighem, M., Rignot, E., Seroussi, H., Larour, E., Ben Dhia, H., and Aubry, D.: Spatial patterns of basal drag inferred using control methods from a full-Stokes and simpler models for Pine Island Glacier, West Antarctica, *Geophys. Res. Lett.*, 37, L14502, doi:10.1029/2010GL043853, 2010.
- Motyka, R., Hunter, L., Echelmeyer, L., and Connor, C.: Submarine melting at the terminus of a temperate tidewater glacier, Leconte Glacier, Alaska, USA, *Ann. Glaciol.*, 36, 57–65, 2003.
- Mukhopadhyay, S., Ackert Jr., R. P., Pope, A. E., Pollard, D., and DeConto, R. M.: West Antarctic ice sheet fluctuations during the Pliocene from ice elevation constraints, *Earth Planet. Sc. Lett.*, in review, 2012.
- Nicholls, K. W., Osterhus, S., Makinson, K., Gammelsrod, T., and Fahrbach, E.: Ice-ocean processes over the continental shelf of the Southern Weddell Sea, Antarctica: a review, *Rev. Geophys.*, 47, 1–23, 2009.

Description of a hybrid ice sheet-shelf model

D. Pollard and
R. M. DeConto

[Title Page](#)

[Abstract](#)

[Introduction](#)

[Conclusions](#)

[References](#)

[Tables](#)

[Figures](#)

[⏪](#)

[⏩](#)

[◀](#)

[▶](#)

[Back](#)

[Close](#)

[Full Screen / Esc](#)

[Printer-friendly Version](#)

[Interactive Discussion](#)



Nick, F. M., van der Veen, C. J., Vieli, A., and Benn, D. I.: A physically based calving model applied to marine outlet glaciers and implications for the glacier dynamics, *J. Glaciol.*, 56, 199, 781–794, 2010.

Olbers, D. and Hellmer, H.: A box model of circulation and melting in ice shelf caverns, *Ocean Dynam.*, 60, 141–153, 2010.

Pattyn, F.: Antarctic subglacial conditions inferred from a hybrid ice sheet/stream model, *Earth Planet. Sc. Lett.*, 295, 451–461, 2010.

Pattyn, F., Perichon, L., Aschwanden, A., Breuer, B., de Smedt, B., Gagliardini, O., Gudmundsson, G. H., Hindmarsh, R. C. A., Hubbard, A., Johnson, J. V., Kleiner, T., Kononov, Y., Martin, C., Payne, A. J., Pollard, D., Price, S., Rückamp, M., Saito, F., Souček, O., Sugiyama, S., and Zwinger, T.: Benchmark experiments for higher-order and full-Stokes ice sheet models (ISMIP–HOM), *The Cryosphere*, 2, 95–108, doi:10.5194/tc-2-95-2008, 2008.

Pattyn, F., Schoof, C., Perichon, L., Hindmarsh, R. C. A., Bueler, E., de Fleurian, B., Durand, G., Gagliardini, O., Gladstone, R., Goldberg, D., Gudmundsson, G. H., Lee, V., Nick, F. M., Payne, A. J., Pollard, D., Rybak, O., Saito, F., and Vieli, A.: Results of the Marine Ice Sheet Model Intercomparison Project, MISIP, *The Cryosphere Discuss.*, 6, 267–308, doi:10.5194/tcd-6-267-2012, 2012.

Payne, A. J., Holland, P. R., Shepherd, A. P., Rutt, I. C., Jenkins, A., and Joughin, I.: Numerical modeling of ocean-ice interactions under Pine Island Bay’s ice shelf, *J. Geophys. Res.*, 112, C10019, doi:10.1029/2006JC003733, 2007.

Pollard, D. and DeConto, R. M.: Antarctic ice and sediment flux in the Oligocene simulated by a climate-ice sheet-sediment model, *Palaeogeogr. Palaeoclimatol.*, 198, 53–67, 2003.

Pollard, D. and Kasting, J. F.: Climate-ice sheet simulations of Neoproterozoic glaciation before and after collapse to Snowball Earth, in: *The Extreme Proterozoic: Geology, Geochemistry and Climate*, edited by: Jenkins, G., McMenamin, M., McKay, C., and Sohl, L., *Geophysical Monograph 146*, American Geophysical Union, Washington, D. C., 91–105, 2004.

Pollard, D. and DeConto, R. M.: Hysteresis in Cenozoic Antarctic ice sheet variations, *Global Planet. Change*, 45, 9–21, doi:10.1016/j.gloplacha.2004.09.011, 2005.

Pollard, D. and DeConto, R. M.: A coupled ice-sheet/ice-shelf/sediment model applied to a marine-margin flowline: forced and unforced variations, in: *Glacial Sedimentary Processes and Products*, edited by: Hambrey, M. J., Christoffersen, P., Glasser, N. F., and Hubbard, B., *International Association of Sedimentologists Special Publication 39*, Blackwell Publ., Oxford, 37–52, 2007.

Description of a hybrid ice sheet-shelf model

D. Pollard and
R. M. DeConto

[Title Page](#)

[Abstract](#)

[Introduction](#)

[Conclusions](#)

[References](#)

[Tables](#)

[Figures](#)

[⏪](#)

[⏩](#)

[◀](#)

[▶](#)

[Back](#)

[Close](#)

[Full Screen / Esc](#)

[Printer-friendly Version](#)

[Interactive Discussion](#)



- Pollard, D. and DeConto, R. M.: Modelling West Antarctic ice sheet growth and collapse through the past five million years, *Nature*, 458, 329–332, 2009.
- Pollard, D. and DeConto, R. M.: Antarctic Ice Sheet variations in response to changes in ice-shelf oceanic melting, International Glaciological Society (IGS) Symposium on Interactions of Ice Sheets and Glaciers with the Ocean, 5–10 June 2011, Scripps Institution of Oceanography, California, USA, Abstract, 2011.
- Pollard, D. and DeConto, R. M.: A simple inverse method for the distribution of basal sliding coefficients under ice sheets, applied to Antarctica, *The Cryosphere Discuss.*, 6, 1405–1444, doi:10.5194/tcd-6-1405-2012, 2012.
- Pollard, D., DeConto, R. M., and Nyblade, A. A.: Sensitivity of Cenozoic Antarctic ice sheet variations to geothermal heat flux, *Global Planet. Change*, 49, 63–74, 2005.
- Rignot, E., Koppes, M., and Velicogna, I.: Rapid submarine melting of the calving faces of West Greenland glaciers, *Nat. Geosci.*, 3, 187–191, 2010.
- Rignot, E., Mouginot, J., and Scheuchl, B.: Ice flow of the Antarctic Ice Sheet, *Science*, 333, 1428–1430, 2011.
- Ritz, C., Fabre, A., and Letreguilly, A.: Sensitivity of a Greenland ice sheet model to ice flow and ablation parameters: consequences for the evolution through the last climatic cycle, *Clim. Dynam.*, 13, 11–24, 1997.
- Ritz, C., Rommelaere, V., and Dumas, C.: Modeling the evolution of Antarctic ice sheet over the last 420,000 years: implications for altitude changes in the Vostok region, *J. Geophys. Res.*, 106, D23, 31943–31964, 2001.
- Rommelaere, V. and Ritz, C.: A thermomechanical model of ice-shelf flow, *Ann. Glaciol.*, 23, 13–20, 1996.
- Scambos, T. A., Bohlander, J. A., Shuman, C. A., and Skvarca, P.: Glacier acceleration and thinning after ice shelf collapse in the Larsen B embayment, Antarctica, *Geophys. Res. Lett.*, 31, L18402, doi:10.1029/2004GL020670, 2004.
- Schoof, C.: Ice sheet grounding line dynamics: steady states, stability, and hysteresis, *J. Geophys. Res.*, 112, F03S28, doi:10.1029/2006JF000664, 2007.
- Shapiro, N. M. and Ritzwoller, M. H.: Inferring surface heat flux distributions guided by a global seismic model: particular application to Antarctica, *Earth Planet. Sc. Lett.*, 223, 213–224, 2004.
- Smith, N. R., Zhaoqian, D., Kerry, K. R., and Wright, S.: Water masses and circulation in the region of Prydz Bay, Antarctica, *Deep-Sea Res.*, 31(9), 1121–1147, 1984.

Description of a hybrid ice sheet-shelf model

D. Pollard and
R. M. DeConto

[Title Page](#)

[Abstract](#)

[Introduction](#)

[Conclusions](#)

[References](#)

[Tables](#)

[Figures](#)

[⏪](#)

[⏩](#)

[◀](#)

[▶](#)

[Back](#)

[Close](#)

[Full Screen / Esc](#)

[Printer-friendly Version](#)

[Interactive Discussion](#)



- Stern, T. A. and ten Brink, U. S.: Flexural uplift of the Transantarctic Mountains, *J. Geophys. Res.*, 94(B8), 10315–10330, 1989.
- Studinger, M., Bell, R. E., Blankenship, D. D., Finn, C. A., Arko, R. A., Morse, D. L., and Joughin, I.: Subglacial sediments: a regional geological template for ice flow in West Antarctica, *Geophys. Res. Lett.*, 28(18), 3493–3496, 2001.
- 5 Timmermann, R., Le Brocq, A., Deen, T., Domack, E., Dutrieux, P., Galton-Fenzi, B., Hellmer, H., Humbert, A., Jansen, D., Jenkins, A., Lambrecht, A., Makinson, K., Niederjasper, F., Nitsche, F., Nøst, O. A., Smedsrud, L. H., and Smith, W. H. F.: A consistent data set of Antarctic ice sheet topography, cavity geometry, and global bathymetry, *Earth Syst. Sci. Data*, 2, 261–273, doi:10.5194/essd-2-261-2010, 2010.
- 10 Tziperman, E., Abbot, D. S., Ashkenazy, Y., Gildor, H., Pollard, D., Schoof, C. G., and Schrag, D. P.: Continental constriction and sea ice thickness in a Snowball-Earth scenario, *J. Geophys. Res.-Oceans*, 117, doi:10.1029/2011JC007730, in press, 2012.
- van den Berg, J., van de Wal, R. S. W., and Oerlemans, J.: Effects of spatial discretization in ice-sheet modelling using the shallow-ice approximation, *J. Glaciol.*, 52, 176, 89–98, 2006.
- 15 van de Berg, W. J., van den Broeke, M. R., and van Meijgaard, E.: Reassessment of the Antarctic surface mass balance using calibrated output of a regional atmospheric climate model, *J. Geophys. Res.*, 111, D11104, doi:10.1029/2005JD006495, 2006.
- van de Berg, W. J., van den Broeke, M., Ettema, J., van Meijgaard, E., and Kaspar, F.: Significant contribution of insolation to Eemian melting of the Greenland ice sheet, *Nat. Geosci.*, 4, 679–683, 2011.
- 20 van der Veen, C. J.: Response of a marine ice sheet to changes at the grounding line, *Quaternary Res.*, 24, 257–267, 1985.
- Vaughan, D. G., Barnes, D. K. A., Fretwell, P. T., and Bingham, R. G.: Potential seaways across West Antarctica, *Geochem. Geophys. Geosy.*, 12(1), Q10004, doi:10.1029/2011GC003688, 2011.
- 25 Walker, R. T., Dupont, T. K., Holland, D. M., Parizek, B. R., and Alley, R. B.: Initial effects of oceanic warming on a coupled ocean-ice shelf-ice stream system, *Earth Planet. Sc. Lett.*, 287, 483–487, 2009.
- 30 Whitehouse, P. L., Bentley, M. J., and Le Brocq, A. M.: A deglacial model for Antarctica: geological constraints and glaciological modeling as a basis for a new model of Antarctic glacial isostatic adjustment, *Quaternary Sci. Rev.*, 32, 1–24, 2012.

Winkelmann, R., Martin, M. A., Haseloff, M., Albrecht, T., Bueler, E., Khroulev, C., and Levermann, A.: The Potsdam Parallel Ice Sheet Model (PISM-PIK) – Part 1: Model description, *The Cryosphere*, 5, 715–726, doi:10.5194/tc-5-715-2011, 2011.

5 Young, D. A., Wright, A. P., Roberts, J. L., Warner, R. C., Young, N. W., Greenbaum, J. S., Schroeder, D. M., Holt, J. W., Sugden, D. E., Blankenship, D. D., van Ommen, T. D., and Siegert, M. J.: A dynamic early East Antarctic Ice Sheet suggested by ice-covered fjord landscapes, *Nature*, 474, 72–75, 2011.

GMDD

5, 1077–1134, 2012

Description of a hybrid ice sheet-shelf model

D. Pollard and
R. M. DeConto

Title Page

Abstract

Introduction

Conclusions

References

Tables

Figures



Back

Close

Full Screen / Esc

Printer-friendly Version

Interactive Discussion



Table 1. Model symbols and nominal values.

x, y	Orthogonal horizontal coordinates (m)
z	Vertical elevation, increasing upwards from a flat reference plane (m)
z'	Vertical ice model coordinate (0 at ice surface, to 1 at base)
dx	Grid cell size, x or y directions (m)
u, u_i, u_b	Horizontal ice velocities in x direction. u = total, u_i = internal deformation, u_b = basal (ma^{-1})
v, v_i, v_b	Horizontal ice velocities in y direction. v = total, v_i = internal deformation, v_b = basal (ma^{-1})
$\dot{\epsilon}_{ij}$	Strain rate components (a^{-1})
$\dot{\epsilon}$	Effective strain rate, 2nd invariant (a^{-1})
σ_{ij}	Deviatoric stress components (Pa)
σ	Effective stress, 2nd invariant (Pa)
μ	$\frac{1}{2} \dot{\epsilon}^{(1-n)/n} (\dot{\epsilon}^{2/3})$
$\text{LHS}_x, \text{LHS}_y$	Left-hand sides of Eq. (2a,b) (Pa)
τ_{xx}	Along-flow longitudinal stress at grounding line (Pa)
τ_f	Non-buttressed longitudinal stress at grounding line (Pa)
h	Ice thickness (m)
h_s	Ice surface elevation (m)
h_b	Bedrock elevation (m)
h_w	Ocean column thickness (m)
h^{eq}	Ice thickness in bed-equilibrium state (m)
h_b^{eq}	Bedrock elevation in bed-equilibrium state (m)
h_w^{eq}	Ocean column thickness in bed-equilibrium state (m)
f_e	Sub-grid cell-area fraction with ice (0 to 1)
h_e	Sub-grid ice thickness within cell-area fraction f_e (m)
h_g	Ice thickness at grounding line (m)
T	Ice temperature ($^{\circ}\text{C}$)
T_m	Ice pressure-melting point ($^{\circ}\text{C}$)
T'	Homologous ice temperature (relative to pressure-melting point) ($^{\circ}\text{C}$)
T_b	Basal ice homologous temperature ($^{\circ}\text{C}$)
Q_i	Internal deformational heating ($\text{J a}^{-1} \text{m}^{-3}$)
Q_b	Basal shear heating ($\text{J a}^{-1} \text{m}^{-3}$)
A	Ice rheological coefficient ($\text{a}^{-1} \text{Pa}^{-3}$)
n	Ice rheological exponent (3)
E	Ice flow enhancement factor (1 for SIA, 0.3 for SSA)
C'	Basal sliding coefficient between bed and ice ($\text{ma}^{-1} \text{Pa}^{-2}$)

Description of a hybrid ice sheet-shelf model

D. Pollard and
R. M. DeConto

Title Page

Abstract

Introduction

Conclusions

References

Tables

Figures

⏪

⏩

◀

▶

Back

Close

Full Screen / Esc

Printer-friendly Version

Interactive Discussion

Table 1. Continued.

$C(x, y)$	Basal sliding coefficient for unfrozen beds ($\text{ma}^{-1} \text{Pa}^{-2}$)
C_{froz}	Basal sliding coefficient for no flow ($10^{-20} \text{ma}^{-1} \text{Pa}^{-2}$)
m	Basal sliding exponent (2)
T_r	Threshold temperature in basal sliding (-3°C)
SA	Sub-grid bed topographic slope amplitude
s_{dev}	Sub-grid standard deviation of bathymetry (m)
f_g	Grounded vs. floating fraction for basal drag (0 to 1)
ρ_i	Ice density (910kg m^{-3})
ρ_w	Ocean water density (1028kg m^{-3})
ρ_b	Bedrock density (3370kg m^{-3})
g	Gravitational acceleration (9.81ms^{-2})
c_i	Specific heat of ice ($2009 \text{J kg}^{-1} \text{K}^{-1}$)
c_w	Specific heat of ocean water ($4218 \text{J kg}^{-1} \text{K}^{-1}$)
c_b	Specific heat of bedrock ($1000 \text{J kg}^{-1} \text{K}^{-1}$)
k_i	Thermal conductivity of ice ($2.1 \times 86400 \times 365 \text{J m}^{-1} \text{a}^{-1} \text{K}^{-1}$)
k_b	Thermal conductivity of bed ($3.3 \times 86400 \times 365 \text{J m}^{-1} \text{a}^{-1} \text{K}^{-1}$)
L_f	Latent heat of fusion ($0.335 \times 10^6 \text{J kg}^{-1}$)
q	Bed load (Pa)
w_b	Lithospheric deflection (m)
D	Lithospheric flexural rigidity (10^{25}Nm)
L	Lithospheric flexural length scale ($(D/\rho_b g)^{1/4}$ ($= 1.32 \times 10^5 \text{m}$))
τ	Asthenospheric isostatic relaxation time scale (a)
SMB	Surface mass balance (ma^{-1})
BMB	Basal ice melt (ma^{-1})
OMB	Sub-ice-shelf oceanic melting (ma^{-1})
CMB	Calving loss (ma^{-1})
FMB	Loss due to oceanic melting at vertical faces (ma^{-1})
T_o	Ocean temperature ($^\circ\text{C}$)
T_f	Ocean freezing point ($^\circ\text{C}$)
K_T	Transfer coefficient for sub-ice oceanic melting ($15.77 \text{ma}^{-1} \text{K}^{-1}$)
K	Additional O(1) coefficient for sub-ice oceanic melting
S	Sea level relative to modern (m)
T_a	Annual mean air temperature ($^\circ\text{C}$)
P	Annual mean precipitation rate (ma^{-1} ice equivalent)

Description of a hybrid ice sheet-shelf model

D. Pollard and
R. M. DeConto

Title Page

Abstract

Introduction

Conclusions

References

Tables

Figures

⏪

⏩

◀

▶

Back

Close

Full Screen / Esc

Printer-friendly Version

Interactive Discussion

**Description of a
hybrid ice sheet-shelf
model**D. Pollard and
R. M. DeConto

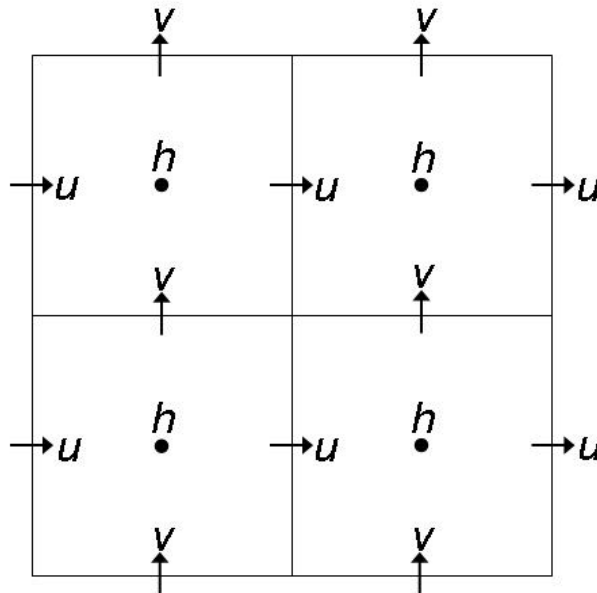
[Title Page](#)[Abstract](#)[Introduction](#)[Conclusions](#)[References](#)[Tables](#)[Figures](#)[◀](#)[▶](#)[◀](#)[▶](#)[Back](#)[Close](#)[Full Screen / Esc](#)[Printer-friendly Version](#)[Interactive Discussion](#)

Fig. 1. Finite-difference staggered grids in the ice sheet-shelf model. h denotes the centers of h -grid boxes, where ice thickness, ice temperatures, and bedrock elevations are calculated. u and v denote the staggered grid points where horizontal velocity components are calculated.

Description of a hybrid ice sheet-shelf model

D. Pollard and
R. M. DeConto

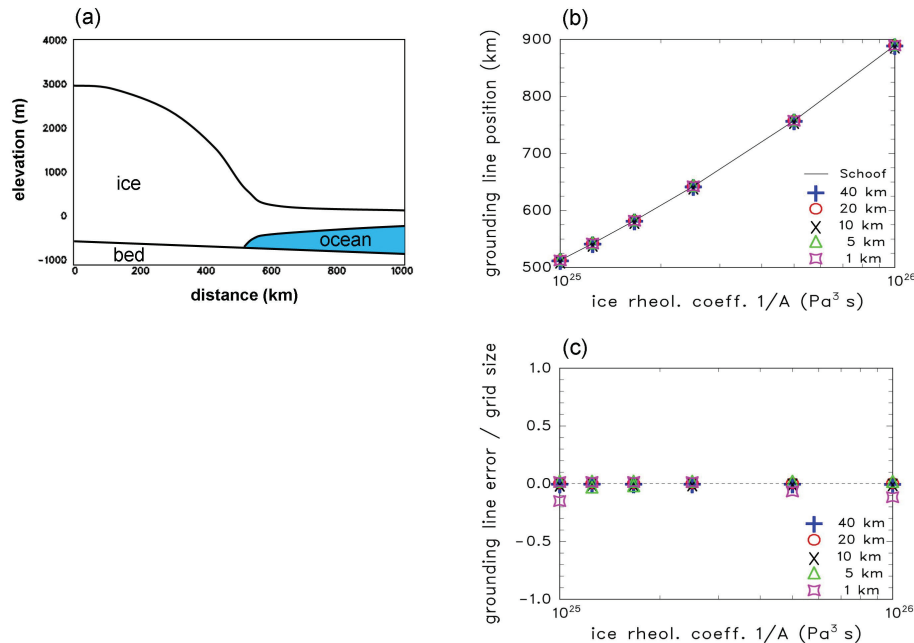


Fig. 2. Idealized flowline model tests, similar to basic MISIMIP (Pattyn et al., 2012), with uniform surface mass balance, an ice divide at the left-hand boundary, a forward-sloping bed into ocean, and using surface-mass-balance increments to q_g (see text). **(a)** Geometry showing sloping bed and ice sheet profiles. **(b)** Model equilibrated grounding-line positions vs. $1/A$ for various grid sizes and initial states. Solid line shows the analytic solution (Schoof, 2007). **(c)** As **(b)** except showing model error (model minus analytic grounding-line position), divided by grid size.

Description of a hybrid ice sheet-shelf model

D. Pollard and
R. M. DeConto

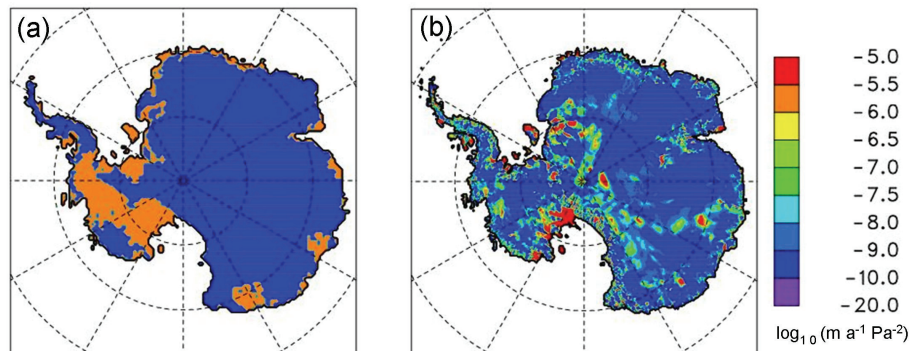


Fig. 3. Basal sliding coefficients $C(x, y)$. **(a)** Simple two-valued map: blue = $10^{-10} \text{ m a}^{-1} \text{ Pa}^{-2}$ (hard bedrock) where modern ice-free rebounded modern bed is above sea level, orange = $10^{-6} \text{ m a}^{-1} \text{ Pa}^{-2}$ (deformable sediment) where below (PD09). **(b)** Deduced from inverse-method fitting to modern ice surface elevations (PD12, with basal temperature and bedrock relief affecting sliding), 20 km resolution.

Title Page

Abstract

Introduction

Conclusions

References

Tables

Figures

⏪

⏩

◀

▶

Back

Close

Full Screen / Esc

Printer-friendly Version

Interactive Discussion

Description of a hybrid ice sheet-shelf model

D. Pollard and
R. M. DeConto

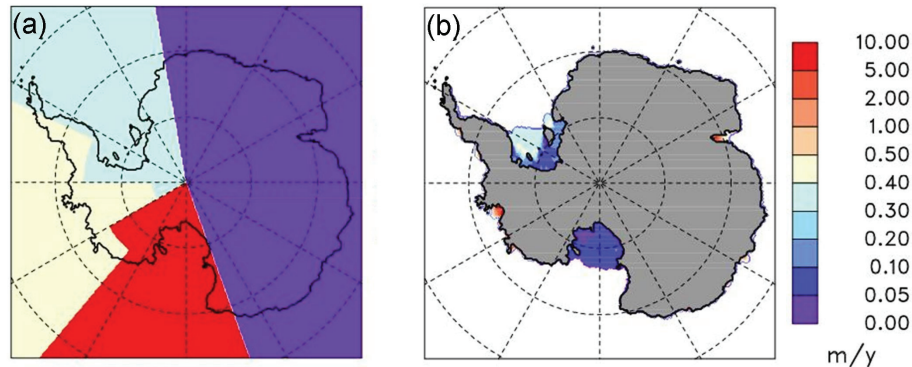


Fig. 4. (a) Sectors used in sub-ice oceanic melt parameterization. *Yellow*: Amundsen and Bellingshausen Seas, and Western Peninsula. *Blue*: Weddell embayment. *Purple*: East Antarctica. *Red*: Ross embayment. (b) Sub-ice oceanic melt rates (m a^{-1}) in modern simulation with 20 km resolution. The average values for each major shelf are reasonable (Nicholls et al., 2009; Olbers and Hellmer, 2010; Dinniman et al. 2011), although somewhat lower for the Ross. Rates are noticeably larger nearer the grounding lines due to the depth dependence of the freezing point T_f in Eq. (17), especially in Pine Island and Prydz Bays, but not noticeably for the flatter Ross Ice Shelf.

[Title Page](#)
[Abstract](#)
[Introduction](#)
[Conclusions](#)
[References](#)
[Tables](#)
[Figures](#)
[⏪](#)
[⏩](#)
[◀](#)
[▶](#)
[Back](#)
[Close](#)
[Full Screen / Esc](#)
[Printer-friendly Version](#)
[Interactive Discussion](#)

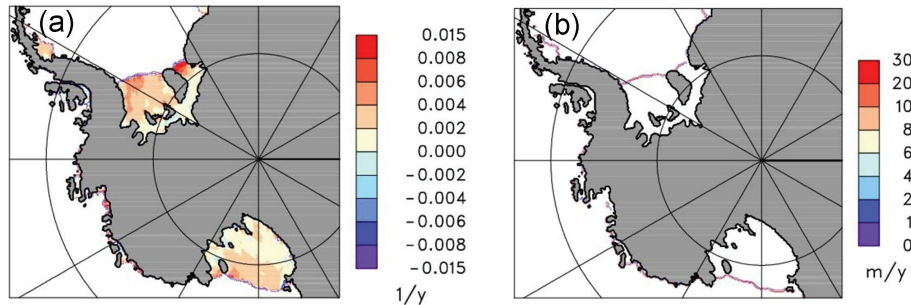


Fig. 5. (a) Divergence $\partial u/\partial x + \partial v/\partial y$ (a^{-1}) of floating ice, in nested 10 km modern simulation with constrained grounding lines and shelf geometry (as in PD12). **(b)** Loss due to calving (CMB, m a^{-1}).

Description of a hybrid ice sheet-shelf model

D. Pollard and
R. M. DeConto

[Title Page](#)

[Abstract](#) [Introduction](#)

[Conclusions](#) [References](#)

[Tables](#) [Figures](#)

[⏪](#) [⏩](#)

[◀](#) [▶](#)

[Back](#) [Close](#)

[Full Screen / Esc](#)

[Printer-friendly Version](#)

[Interactive Discussion](#)



Description of a hybrid ice sheet-shelf model

D. Pollard and
R. M. DeConto

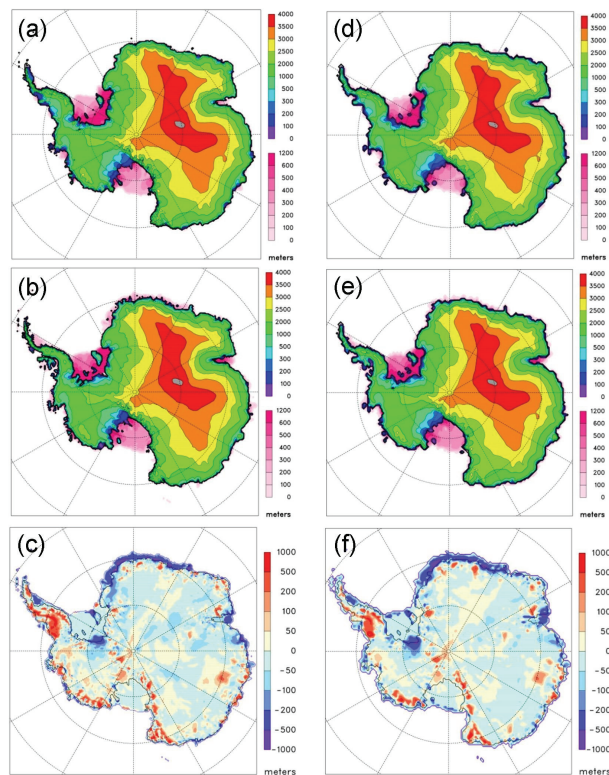


Fig. 6. Modern grounded ice surface elevations (upper scale, meters) and floating ice thicknesses (lower scale, meters). **(a)** Observed (Le Brocq et al., 2011), averaged to 20 km resolution. **(b)** Model, 20 km resolution, with basal sliding coefficient map from inverse method described in PD12. **(c)** Difference in surface elevations, 20 km model minus observed. **(d–f):** As **(a–c)** except 40 km resolution.

[Title Page](#)
[Abstract](#)
[Introduction](#)
[Conclusions](#)
[References](#)
[Tables](#)
[Figures](#)
[⏪](#)
[⏩](#)
[◀](#)
[▶](#)
[Back](#)
[Close](#)
[Full Screen / Esc](#)
[Printer-friendly Version](#)
[Interactive Discussion](#)

Description of a hybrid ice sheet-shelf model

D. Pollard and
R. M. DeConto

Title Page

Abstract

Introduction

Conclusions

References

Tables

Figures



Back

Close

Full Screen / Esc

Printer-friendly Version

Interactive Discussion

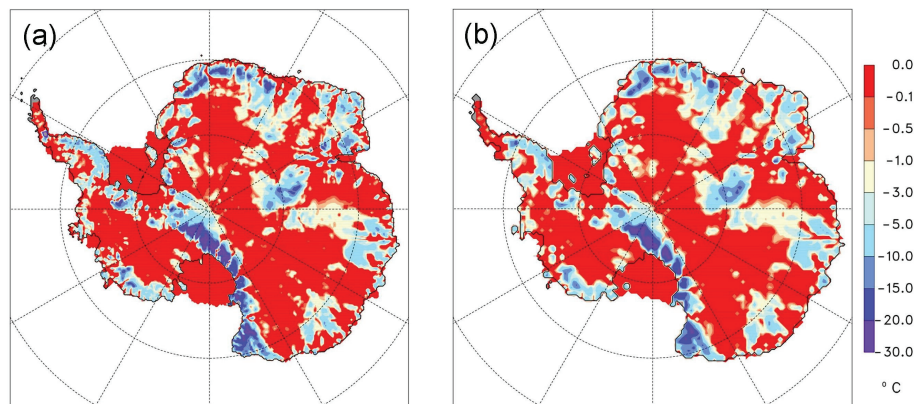


Fig. 7. Modern basal homologous temperature (relative to pressure melting point), °C. **(a)** 20 km resolution, model as in Fig. 6(b,c). **(b)** 40 km resolution, model as in Fig. 6(e,f).

**Description of a
hybrid ice sheet-shelf
model**D. Pollard and
R. M. DeConto

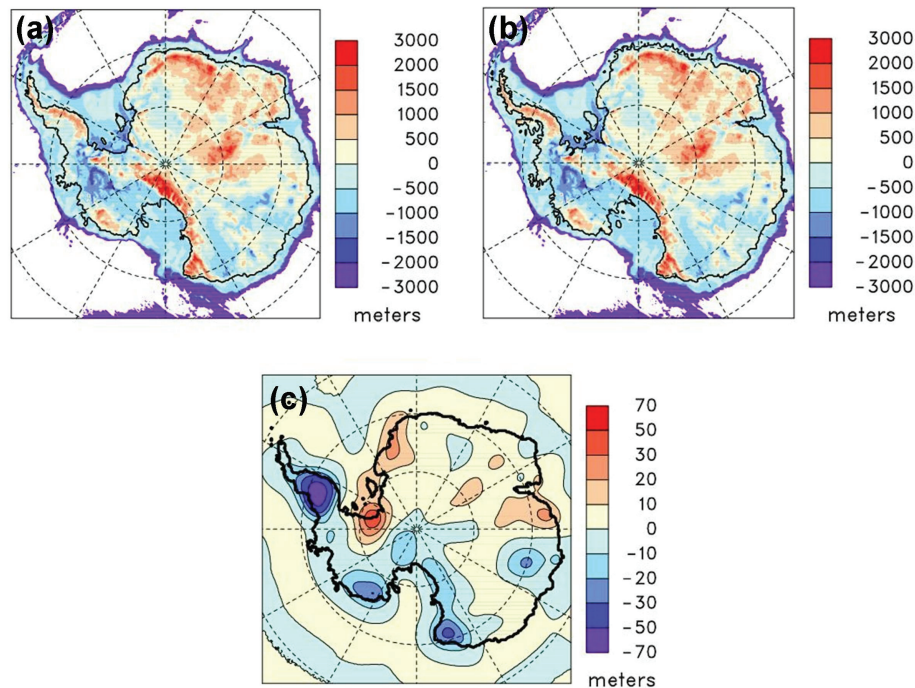


Fig. 8. (a) Bed elevations, meters, in modern simulation at 20 km resolution. (b) Observed modern bed elevations, meters (Le Brocq et al., 2011). (c) Difference, model minus observed.

[Title Page](#)[Abstract](#)[Introduction](#)[Conclusions](#)[References](#)[Tables](#)[Figures](#)[◀](#)[▶](#)[◀](#)[▶](#)[Back](#)[Close](#)[Full Screen / Esc](#)[Printer-friendly Version](#)[Interactive Discussion](#)

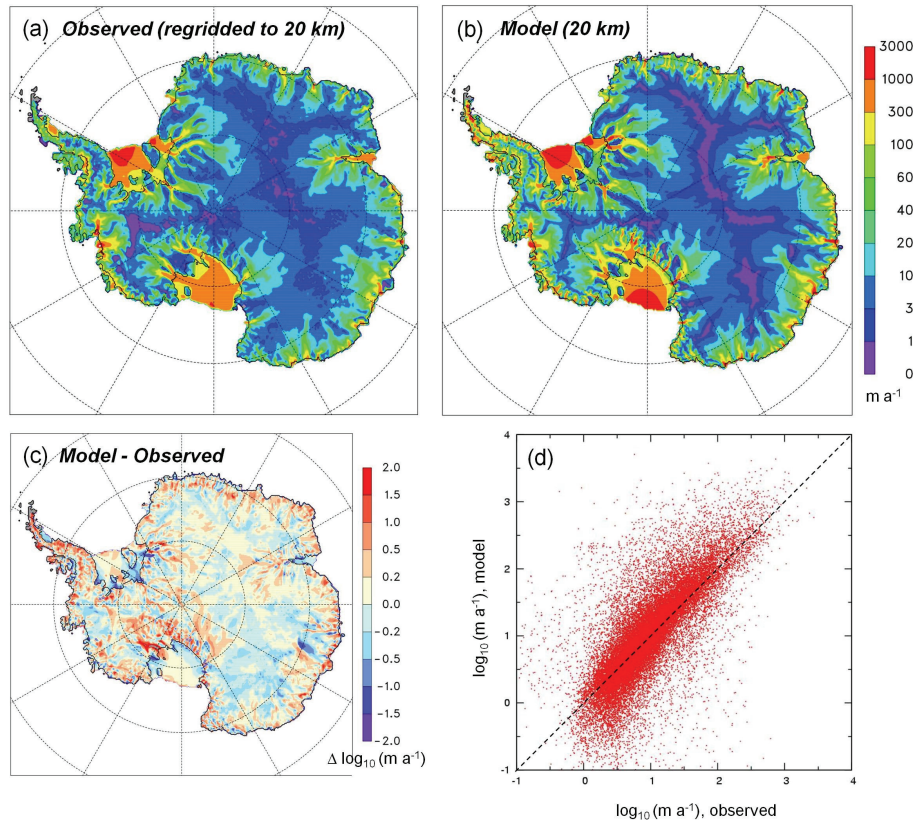


Fig. 9. (a) Observed surface ice velocity (Rignot et al., 2011), averaged here to 20 km model cells, m a^{-1} . (b) Model surface ice velocity, m a^{-1} , in modern simulation at 20 km resolution. (c) Model minus observed velocity, difference in $\log_{10}(\text{m a}^{-1})$, i.e., $\log_{10}(v_{\text{model}}/v_{\text{observed}})$, with imposed minimum of 2 m a^{-1} . (d) scatter plot of observed vs. model velocities ($\log_{10}(\text{m a}^{-1})$) for each 20 km grid cell with grounded ice. The same figure appears in PD12 (Fig. C1).

Description of a hybrid ice sheet-shelf model

D. Pollard and
R. M. DeConto

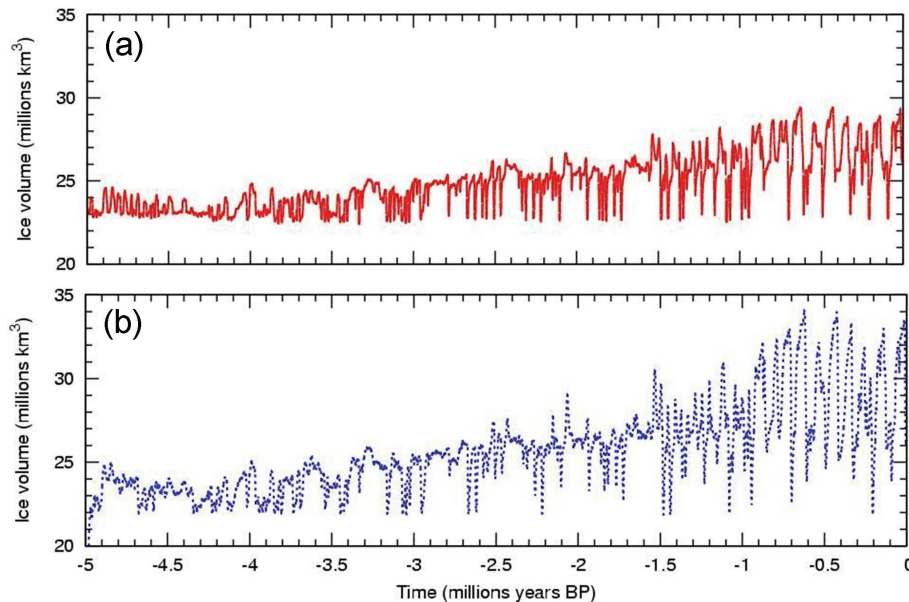


Fig. 10. Time series of total Antarctic ice volume (10^6 km^3) over the last 5 million yr, in simulations with parameterized climatic and oceanic forcing dependent mainly on deep-sea-core $\delta^{18}\text{O}$, and slightly on austral summer insolation, with 40 km model resolution. **(a)** Current model, with inverse-derived basal sliding coefficients $C(x, y)$, and value on continental shelves = $10^{-5} \text{ ma}^{-1} \text{ Pa}^{-2}$. **(b)** Earlier model version as in PD09 (their Fig. 3a) with simple two-valued $C(x, y)$ and continental-shelf value = $10^{-6} \text{ ma}^{-1} \text{ Pa}^{-2}$.

[Title Page](#)
[Abstract](#)
[Introduction](#)
[Conclusions](#)
[References](#)
[Tables](#)
[Figures](#)
[⏪](#)
[⏩](#)
[◀](#)
[▶](#)
[Back](#)
[Close](#)
[Full Screen / Esc](#)
[Printer-friendly Version](#)
[Interactive Discussion](#)

Description of a hybrid ice sheet-shelf model

D. Pollard and
R. M. DeConto

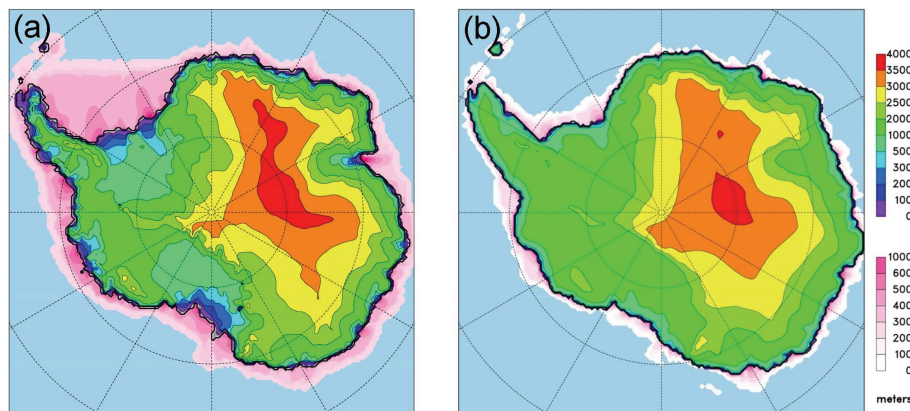


Fig. 11. Grounded ice surface elevations (upper scale, meters) and floating ice thicknesses (lower scale, meters), at 15 kyr BP in simulations of the last 5 million yr. **(a)** Current model with inverse-derived basal sliding coefficients $C(x, y)$, and value on continental shelves = $10^{-5} \text{ m a}^{-1} \text{ Pa}^{-2}$ (as Fig. 10a). **(b)** As in PD09, with simple two-valued $C(x, y)$ and continental-shelf value = $10^{-6} \text{ m a}^{-1} \text{ Pa}^{-2}$ (as Fig. 10b).

[Title Page](#)
[Abstract](#)
[Introduction](#)
[Conclusions](#)
[References](#)
[Tables](#)
[Figures](#)
[⏪](#)
[⏩](#)
[◀](#)
[▶](#)
[Back](#)
[Close](#)
[Full Screen / Esc](#)
[Printer-friendly Version](#)
[Interactive Discussion](#)
